

Transparent ultrasound transducer for photoacoustic imaging

Making a 2x2 array using PVDF coated with ITO

Amber Plakke

s2314819

Biomedical Engineering

Bachelor assignment BMPI

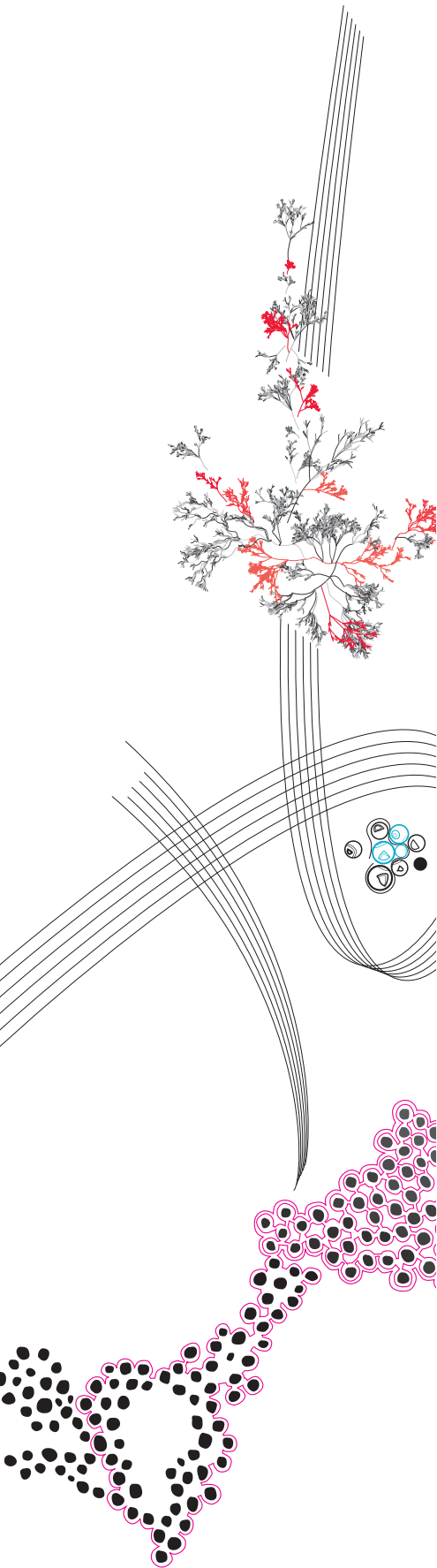
July 11, 2022

Examiners

Chair: Prof. Dr. Ir. W. Steenbergen

Daily supervisor: Dr. F. Kalloor Joseph

External: Dr. M. Morales Masis



Abstract

Circulating Tumor Cells (CTC) are cells that come from a tumor, but are migrating through the body via the bloodstream. In this way, the cancer is spread further through the body.

To make this migrating CTC's visible in the skin's blood vessels, photoacoustic imaging (PAI) can be used. Therefore a transparent transducer array is needed, in this case the light can be sent through the transducer and the sound wave could be detected at the same location. Further on, a large area could be imaged when using an array configuration. Currently all commercially available transducers use opaque piezoelectric material.

In this work, a transparent ultrasound transducer 2x2 array is developed using transparent polyvinylidene fluoride (PVDF) piezoelectric material with a coating of tin oxide (ITO). A protocol is made for selectively removing ITO and the process of making the transducer is described. There are four active regions on the transducer that are tested in an experimental setup. The active regions could be measured separately, and the active region where the acoustic waves are sent on could be distinguished from the other regions. Further research should be done to develop a more accurate data processing method for determining the location of the CTC's. Further on, a way of measuring all regions at the same time should be developed.

Samenvatting

Circulerende tumor cellen (CTC) zijn cellen afkomstig van een tumor, maar migreren door de bloedvaten naar andere delen van het lichaam. Op deze manier wordt de kanker verder verspreid in het lichaam.

Om deze migrerende CTC's zichtbaar te maken in de bloedvaten van de huid, kan photoacoustic imaging (PAI) worden gebruikt. Hiervoor is een transparante transducer array nodig. Op deze manier kan het licht door de transducer worden geschonden op de huid, vervolgens kunnen de geluidsgolven opgevangen worden op diezelfde plek. Verder kan een groter oppervlakte bekeken worden als er gebruik wordt gemaakt van een array configuratie. Op dit moment gebruiken alle commerciële beschikbare transducers ondoorzichtig piezo-elektrisch materiaal.

In deze thesis is een transparante ultrageluid transducer 2x2 array ontwikkeld. Hierbij is gebruik gemaakt van polyvinylidene fluoride (PVDF) piezo-elektrisch materiaal met een coating van tin oxide (ITO) dat elektriciteit geleid. Er is een protocol opgesteld voor het selectief verwijderen van ITO en de constructie van de transparante transducer is beschreven. Er zijn vier actieve regio's op de transducer, elektrodes, die getest zijn in een experimentele opstelling. De actieve regio's worden apart van elkaar gemeten en de actieve regio waar de geluidsgolven op wordt gefocuseerd kan onderscheiden worden van de andere regio's. Meer onderzoek zou gedaan kunnen worden om een accuratere manier van data verwerking te kunnen verkrijgen, met als doel de locaties van de CTC's vast te kunnen stellen. Verder zou er een manier gevonden moeten worden om alle regio's tegelijkertijd te kunnen meten.

Contents

1	Introduction	6
1.1	Photoacoustic imaging	6
1.2	PAI melanosome CTC's and blood	6
1.3	Transparent Transducers	7
1.4	Transparent Transducers PVDF ITO	9
1.5	Research goal and research questions	10
2	Design Aspects	11
2.1	Imaging Depth	11
2.2	Substrate	11
2.2.1	Properties PMMA	11
2.2.2	Shape substrate	12
2.3	Attachment	13
2.4	PVDF	13
2.5	ITO	14
2.6	Frequency Response	14
2.7	Dimensions Transducer	14
3	Selectively removing ITO	15
3.1	Removing ITO	15
3.2	Etching time	16
3.2.1	Materials	16
3.2.2	Method	16
3.2.3	Results and discussion	16
3.3	Photoresist Dry Film	17
3.3.1	Applying the Photoresist dry film (PDF)	17
3.4	Removing PDF	18
3.4.1	Materials	18
3.4.2	Method	18
3.4.3	Results and discussion	19
3.5	Final Procedure	21
3.5.1	Material	21
3.5.2	Method	21
4	Making the Transducer	23
4.1	Materials	23
4.2	Method	23
4.2.1	PVDF film	23
4.2.2	Substrate and attachment	24
4.3	Electronics	24
5	Characterizing and Testing	26
5.1	Testing the effect of the process of ITO removal on the performance	26
5.2	Testing the transducer	29
5.2.1	The setup	29
5.2.2	First test with Prototype 1	30

5.2.3	Focusing on multiple regions	32
5.2.4	Inverting the transparent transducer 180 degrees	33
5.2.5	Swapping the cables in the switch box	34
5.2.6	Prototype 2	34
5.2.7	Grounding the transparent transducer to the power supply ground	35
5.2.8	Connecting 1 wire to earth	37
5.2.9	Subtraction of the signals	37
5.3	Prototype 3	39
6	Conclusions and outlook	41
6.1	Conclusions	41
6.1.1	Transducer development	41
6.1.2	Testing transparent transducer	41
6.2	Outlook	42
A	Ground swapped	47
B	Figures regarding grounding	49
C	Subtract in oscilloscope	54
D	Impedance measurement	58

Chapter 1 Introduction

Metastasis is the cause of 90% of cancer-related deaths [1]. The tumor cells are mostly spread through the blood and then called Circulating Tumor Cells (CTC's). CTC's are important indicators of the severity of the metastasis and the effectiveness of the cancer treatment. To make these migrating CTC's visible in blood vessels in the skin, photo-acoustic imaging (PAI) can be used [1].

1.1 Photoacoustic imaging

With photo-acoustic imaging (PAI) the high-contrast and spectroscopic-based specificity of optical imaging is combined with the high spatial resolution of ultrasound imaging. This acquires structural and functional information from most soft tissues [2]. A laser beam with a specific wavelength is aimed at the tissue. The laser pulses should be very short with a high intensity. This has to do with the thermal relaxation time of the tissue. The thermal relaxation time is the time that it takes an object to diffuse 63% of the incident thermal energy to the adjacent tissue. This time is different for different objects because it is related to size and optical absorption [3]. When pulses shorter than the thermal relaxation time are sent, the heat will stay at the place in the tissue the laser was aimed at. This causes effective and selective photothermolysis of the absorbing cells. The thermal relaxation time for melanosomes (size 0.5-1.0 μm) is 1 μs and for a blood vessel (size 50, 100, 200 μm) it is 1, 5, 20 ms respectively [4]. Hence, using a nanosecond pulsed laser source, the condition for thermal confinement is satisfied. The laser energy is absorbed by the tissue and converted to heat. This gives a local pressure rise that causes high frequency ultrasound waves, which can be detected with the transducer [5]. When measuring at multiple spatial locations, a photoacoustic image of the target tissue can be formed.

In order to destroy the absorbers inside the CTC, the energy of the laser pulse should be higher. So the absorbers are heated beyond the temperature for explosive evaporation, the CTC is then photomechanically killed. In this way the amount of CTC's in the blood can be decreased and may even prevent metastasis to form tumors. Becoming immune for this kind of therapy won't happen, because the cells are killed photomechanically. Further on, other molecules would not sustain damage because the therapy is highly focused on the absorbers in the CTC's, for example melanosomes in melanoma CTC's. However, high temperature rises can give necrosis to the tissue. Olds et al. investigated 2 different laser frequencies, 10 Hz and 30 Hz, on mouse skin. They found that with the higher frequency laser, necrosis would occur. Further on, necrosis could be prevented by cooling the tissue [6].

Commercially available transducers use opaque piezoelectric material. In order to deliver the laser light to the tissue, transducers with a hole in the center were developed [7]. But the focusing ability and the acoustic sensitivity of the sensor will be reduced due to this hole [2] and the imaging surface is limited. A transducer that is fully transparent could solve this issue, making photoacoustic imaging more sensitive.

1.2 PAI melanosome CTC's and blood

Melanoma, also known as skin cancer, is a type of cancer with high metastatic potential. When the metastasis begins, the clinical outcomes are poor, with a median survival rate of only 6 months [8]. He et al. investigated melanoma CTC's with PAI [1]. The melanoma CTC's had a 5 times higher amplitude for absorbance compared to the background if a wavelength of 1064 nm was used. With 532 nm the difference between a red blood cell (RBC) and a melanoma CTC is not that clear because of the similar absorption coefficients for melanosome and Hb at 532 nm. When using 532 nm and 1064 nm the particles could be

distinguished, see Figure 1.1. CTC's were monitored and a therapy for killing the CTC's was used. Only 1 out of the 6 mice developed a tumor after the therapy and this tumor formation took longer than the control group. It could be that some CTC's are missed, which could be prevented with a higher repetition time.

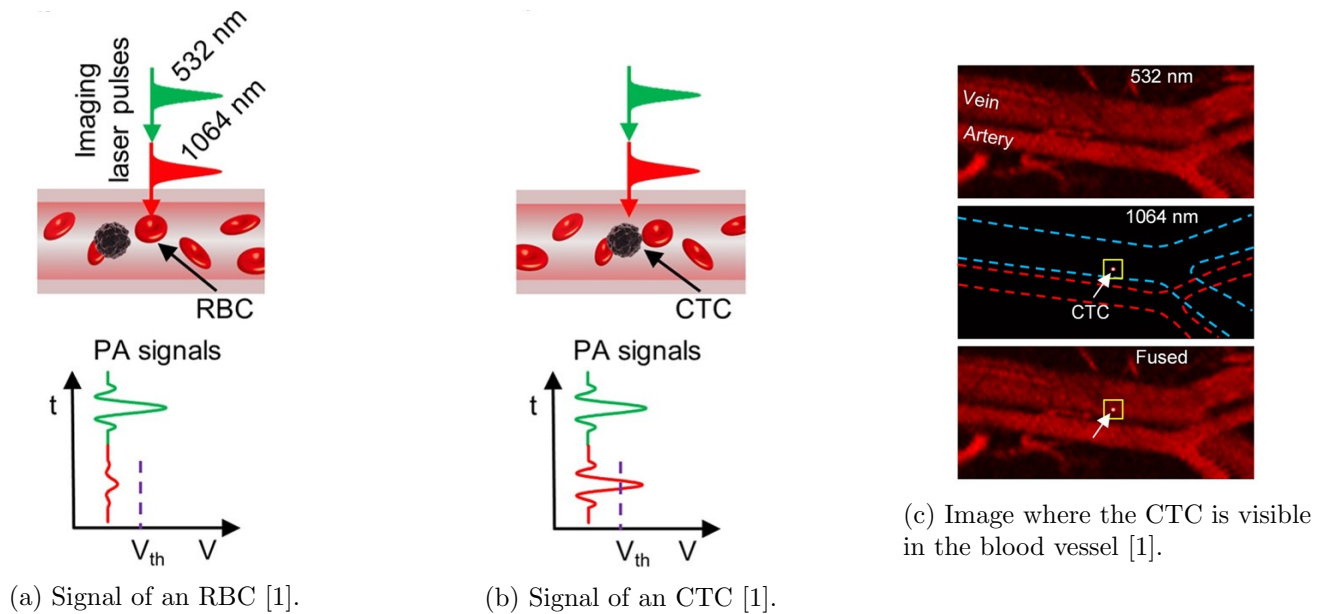


Figure 1.1: Imaging melanoma CTC in a blood vessel using 532 nm and 1064 nm wavelength lasers [1].

This technique could also be used for other types of CTC's, but these cells will need a different wavelength that is suitable for their absorbers. However, most other CTC's do not have such a good absorber with a good contrast like melanoma, therefore molecular probes can be used to mark CTC's [8]. In this way CTC's can be made visible using PAI, however killing the melanoma CTC's is based on breaking the melanoma and that causes the CTC to break down. So whether this technique can be used to kill more cells is a question very specific for each type of tumor cell. Marking CTC's has been done before, for example with breast cancer cells and prostate cancer cells. Magnetic nanoparticles are found in breast cancer cells, but to improve the detection gold plated carbon nanotubes conjugated with folic acid were used as a second contrast agent [9]. With these absorbers good contrast was created and breast cancer CTC's were imaged using PAI. For prostate cancer CTC's, gold nanoparticles have been attached to the prostate cancer cells [10]. This gave a good contrast such that prostate CTC's could be imaged using PAI.

1.3 Transparent Transducers

For imaging CTC's with PAI a transparent transducer is required, in this case the light can be sent through the transducer and the sound wave could be detected on the same location. Further on, it is convenient if a large skin window (10x10 cm), like the back, can be imaged. Therefore it is not sufficient to perform photoacoustic imaging the classical way, by placing the laser and the detector under an angle, like in Figure 1.2.

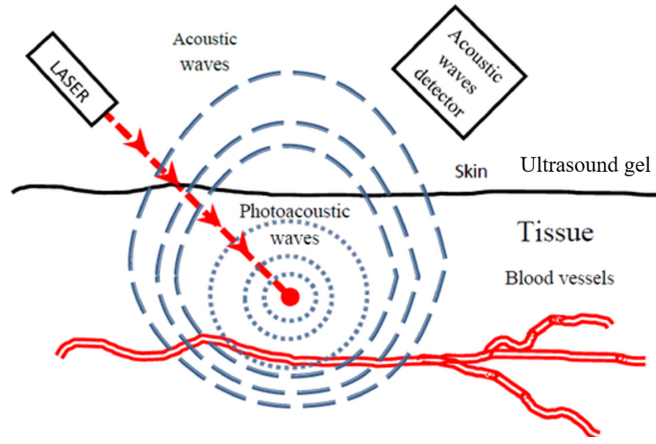


Figure 1.2: Photoacoustic imaging, by placing the laser source and the detector under an angle [11].

Transparent transducers were developed in the past with different techniques and materials. In this section, they will be discussed briefly. There are three categories of transparent transducers that were investigated in the past [2]:

- **Transparent Optics-Based Ultrasound Transducers**

In this type of transducers, optical resonance is used to detect PA signals. This is done without contact and could also be done without using an acoustic coupling medium. The ultrasound waves are converted to optical properties through optical interference or resonance.

- **Fary-Perot interferometer (FPI) sensors;** Fary-Perot based sensors work based on the following principles. With short laserpulses (ns) broadband high-frequency ultrasound waves can be formed in certain materials, the transmitter coating of the sensor, see Figure 1.3. Then there are two dielectric mirrors which are separated from each other by a spacer. This cavity can contain parlylene C for example [12]. The acoustic waves will make the diameter of this spacer change. This change in thickness will also change the way the beams are reflected in the mirrors, so in this way the change in thickness could be measured [12] [13] [14]. The diameter and thickness of the film can be changed in order to change the frequency or the sensitivity of the transducer. An FP sensor with a polymer film as the spacer can give broad frequency response (several tens of megahertz) and have a high sensitivity which is comparable with piezoelectric-based sensors.

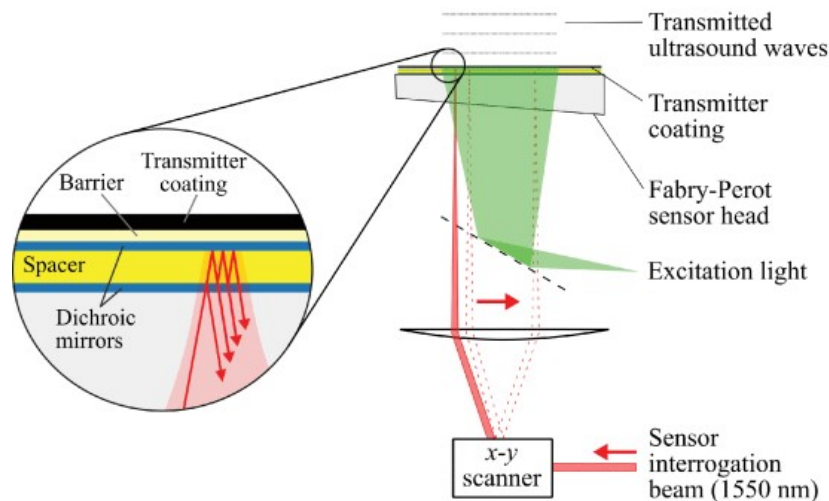


Figure 1.3: an example of a Fary-Perot interferometer, used for acoustic waves [12]

- **Micro Ring Resonator (MRR);** MRR is made of a close bus waveguide and a ring-shaped resonator separated by a low dielectric gap [2] [15]. The bus waveguide functions as the in- and output ports, the low dielectric gap couples the bus waveguide and the ring-shaped resonator, by evanescently tunneling across this gap. The ultrasound wave causes a deformation in the ring-shaped resonator. This causes a change in the effective optical path length, which will cause

a shift in resonance frequency. These changes will be detected and the characteristics of this ultrasound wave can be determined.

- **Grating-based sensors**; This sensor is composed of Bragg gratings and a laser cavity [2]. The ultrasound wave will hit the sensor, this stress causes birefringence. This birefringence will cause a frequency shift, this can be detected. These sensors have a large bandwidth.

- **Transparent Piezoelectric-Based US Sensors**

This type of sensor consists of an active piezoelectric layer, this material can convert pressure into electrical signals. The layer should be coated with top and bottom electrodes in order to transmit or receive signals. Indium tin oxide (ITO) is commonly used in this type of sensors as a transparent electrode [2].

- **ITO coated PVDF film**; PVDF is a highly nonreactive polymer, has good optical properties and low acoustic impedance and is a good material to use [2]. Due to its low acoustic impedance backing and matching layers are unnecessary. In 1.4 ITO coated PVDF will be discussed more in detail.
- **Lithium niobite (LN)**; LN is a single-crystal material, which can be used as a piezoelectric material. In the range of 350 nm to 5200 nm LN has an optical transmittance of 0.8 [2].
- **PMN-PT ceramics**; PMN-PT ceramic is a new developed piezoelectric ceramic [2].

- **Transparent Capacitive Micromachined Ultrasonic Transducers**

These types of transducers are made with two membrane plates [2] [16]. The first membrane has a bottom electrode. The other membrane is placed on top with the top electrode. When the ultrasound wave reaches the top electrode, a vibration is triggered which changes the capacitance of the transducer. Detection can then be done by measuring the change in capacitance of the transducer over time. This does not require a matching layer for matching the acoustic impedance.

1.4 Transparent Transducers PVDF ITO

Niederhauser et al. compared an ITO coated PVDF transducer with an Aluminum coated PVDF transducer [17]. The PVDF foil had a thickness of 40 μm and was sputtered with ITO (thickness of 200 nm). The coated foil was placed on polymethyl methacrylate (PMMA) with a thickness of 2 cm. Glycerin was used for adhesion between the materials. For the protection of the film a clingfilm was placed on top and glycerin was placed in between the films for adhesion. They proved that ITO and Aluminum had a similar sensitivity, and therefore ITO can be adequately used in transparent transducers.

Fang et al. developed a focused transducer [18]. The PVDF film had a thickness of 9 μm and was trimmed with a film cutter. The substrate was a concave glass lens, the PVDF was laminated onto that. The film was stretched and formed so that it would fit in the lens. The ITO (thickness of 400 nm) and chrome (thickness 15 nm)/ copper (thickness 200 nm) are deposited onto PVDF film on the convex side. The film is then glued onto the spherical surface on the concave glass, this is done with UV epoxy. This gave an optical transmittance of the transducer of $\sim 60\%$ at the wavelength of 532 nm. The center frequency was 24 MHz and the bandwidth was 26 MHz.

Blumenröter et al. made a transparent transducer by placing the film between two substrates [19]. On both sides the PVDF was sputtered with ITO, the shape of the ITO was cut out of a metal plate to create a mask during the sputtering. The shape was chosen smoothly without sharp corners to prevent voltage spikes and reflections inside the electrodes. The PVDF was glued in between two sheets of PMMA, the optical adhesive that was used was 85V, Norland Products. The backing layer was 5 mm thick PMMA and the fronting layer was 0.5 mm thick. The transmission through the coated film is above 60% for most parts of the visible wavelength range.

The transducer that Snook et al. designed was made with a backing of unloaded EPO-TEK 301 epoxy, has an impedance of 3.15 MRayl [20]. No matching layer was used due to the low acoustic impedance of PVDF with was 3.89 MRayl. The thickness of the materials were less than the required $\lambda/2$ because the center frequency will be down-shifted by the load of backing and matching as well as electrodes. The transducer

had a poor sensitivity in comparison to the other three transducers that have been tested.

Liu et al. investigated a transducer without gluing it onto a substrate [21]. PVDF with a thickness of 110 μm was used. This film was covered in silver and cut into 3 by 2 cm^2 pieces. Then the silver coating was removed from the film and ITO was sputtered onto the film. In this research there was no substrate to which the film was connected, instead the film was placed in a 3D printed construction. They found out that the thickness of the ITO coating matter for the transmittance, 150 nm, exhibited a higher transmittance at 532 nm than other thicknesses.

1.5 Research goal and research questions

The goal of the research is to develop a transparent ultrasound transducer 2x2 array from PVDF coated with ITO and to test its acoustic and electrical characteristics.

How to make a transparent ultrasound transducer two by two array using PVDF coated with ITO?

- What kind of substrate?
- What kind of adhesive?
- What dimension of substrate (Thickness, Size, Shape)?
- How big should the electrodes be, how to make the shape?
- How to selectively remove ITO?
 - What concentration HCl should be used?
 - How to cover the ITO that must be kept?
 - How long should the film be washed for the ITO to be removed?
- What kind of experiments should be done to characterize the transducer and test how it functions?

Chapter 2 Design Aspects

In this chapter, the design aspects of the transducer will be discussed.

A two by two transducer array will be made, with four active sides. This is done by using ITO coated PVDF film. The ITO will be selectively removed, such that it can function as electrodes. See Figure 2.1.

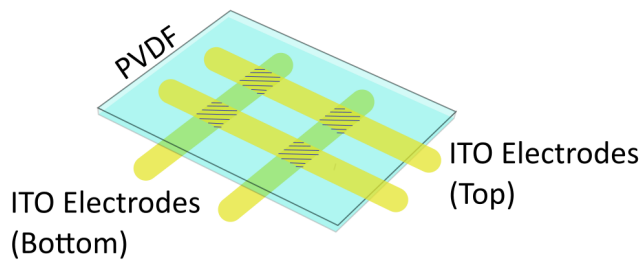


Figure 2.1: PVDF film with ITO electrodes, the four element transducer.

2.1 Imaging Depth

The depth of superficial blood-vessels on the upper limb is between 2.1 and 3.1 mm [22]. The skin itself has a varying thickness of 1.5- 4.0 mm [23]. So if the laser can reach about 4.0 mm the imaging depth should be sufficient for imaging CTC's.

2.2 Substrate

The substrates mentioned in 1.4 were mainly glass or PMMA. The impedance of quartz glass is 13.1 MRayl, glass ceramics 16.5 MRayl and of PMMA 3.32 MRayl [24] [25]. The impedance of PMMA is sufficiently smaller than glass and more close to the impedance of PVDF. Therefore less reflections occur at the interface between those materials. Therefore PMMA is considered more suitable as a substrate for the transducer.

2.2.1 Properties PMMA

The speed of sound in PMMA is 2757 m/s and the acoustic impedance is 3.32 MRayl [25]. The optical transmittance of PMMA is around 92%, see Figure 2.2 [26]. The speed of sound in water is 1486 m/s and the acoustic impedance is 1.49 MRayl [27].

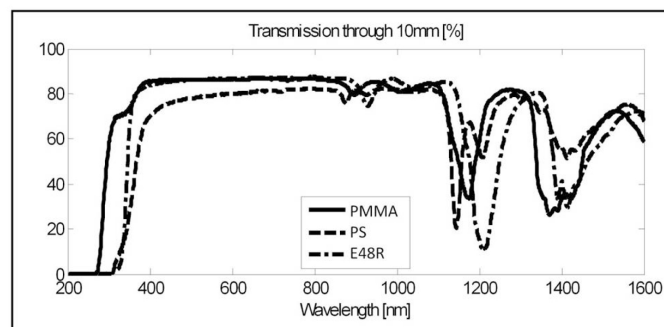


Figure 2.2: Optical transmission in PMMA with a thickness of 10 mm [26].

2.2.2 Shape substrate

To resolve the internal reflection inside the substrate, the substrate can be formed into a shape that reflects the acoustic waves away from the piezoelectric film [28]. In Figure 2.3 this shape has been drawn. With T the basis thickness of the substrate, x the thickness of the triangle shape on top of that, S is the distance at which the reflected acoustic wave should leave the transducer with respect to the piezoelectric film and l is the length of the transducer perpendicular to the flow direction of the blood. In this case it is assumed that the CTC's are in the middle position and the laser only points at that specific point. The laser beam (red) falls onto the substrate with an angle i . The angle (r) of the refracted laser light is the same as the angle of the reflected acoustic wave (green). The angle θ is the angle of the triangle part.

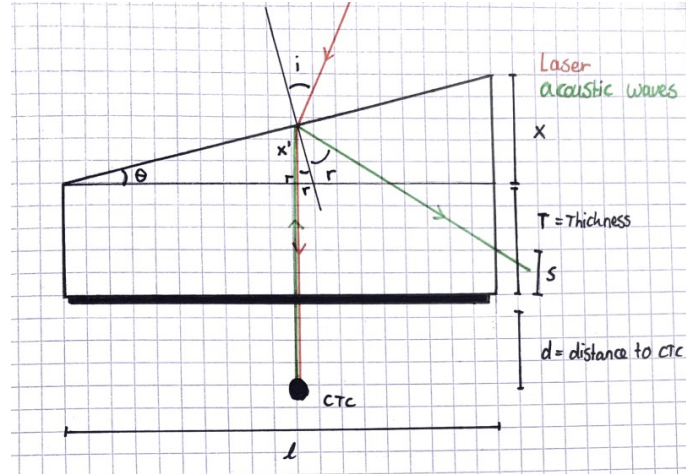


Figure 2.3: Side view: shape of the transducer that reflects acoustic waves away from the surface.

From goniometrics follows: $90^\circ - \theta = 90^\circ - r$ so, $\theta = r$

Reflection law states:

$$\frac{\sin(i)}{\sin(r)} = \frac{\mu_1}{\mu_2} \quad (2.1)$$

In Table 2.1 refractive indices are given for materials. With this information the angle of incident for the laser beam could be calculated:

$$\sin(i) = \frac{\mu_2}{\mu_1} \cdot \sin(r) = \frac{\mu_{PMMA}}{\mu_{Water}} \cdot \sin(\theta) \quad (2.2)$$

Medium	Refractive index (μ)
PMMA	1.48 [29]
Water	1.333 [30]
PVDF	1.426 [31]
NOA 85V	1.46 [32]

Table 2.1: Refractive indices, with NOA 85V that will function as epoxy for attachment.

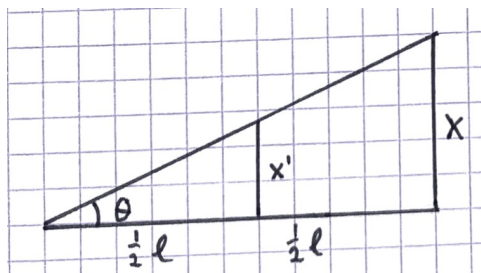


Figure 2.4: Top part of the transducer

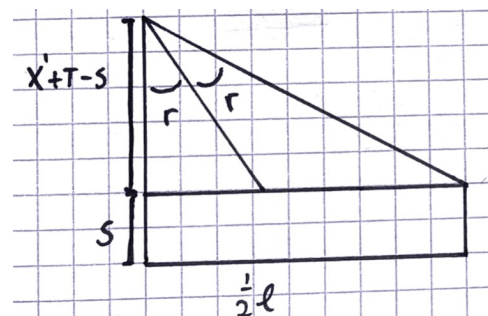


Figure 2.5: Half the transducer

From Figure 2.4 x' can be calculated:

$$x' = \frac{\frac{1}{2} \cdot l \cdot x}{l} \quad (2.3)$$

From Figure 2.5 follows:

$$\tan(2\theta) = \frac{\frac{1}{2}l}{x' + T - S} \quad (2.4)$$

2.3 Attachment

One of the epoxies that was mentioned was NOA85V, this epoxy will cure when exposed to UV or visible light [33]. The curing time depends on the thickness and the amount of UV light. The viscosity is 200 cp at 25 degree Celsius. Further on, the optical transmission is good in the range 400-1200 nm which is sufficient for the experiments, see Figure 2.6. The optical transmission in Near Infrared is typical between 650-1000 nm [30].

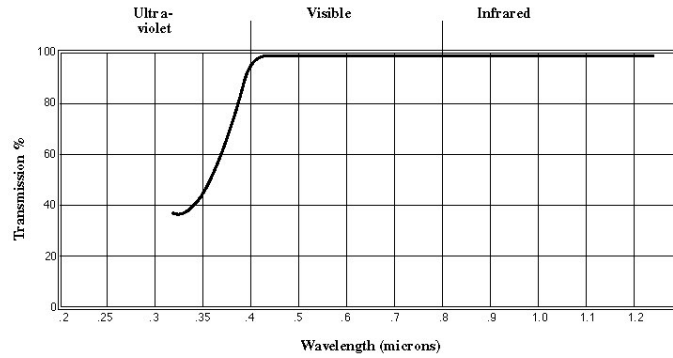


Figure 2.6: Spectral transmission NOA 85V [32].

EPO-TEK 301 was also mentioned; it consists of two components and cures at room temperature. It has a low viscosity (100-200 cps at 23 degree Celsius). The transmission at 23 degree Celsius is $\geq 99\%$ at 382 - 980 nm, $\geq 97\%$ at 980-1640 nm, $\geq 95\%$ at 1640-2040 [34].

Both epoxies have similar properties, like high transmittance and low viscosity. But NOA85V has only one component and will therefore be easier to use, so this epoxy is chosen.

2.4 PVDF

Piezoelectric material converts pressure from the sound waves into a certain voltage and gives electrical signals. Polyvinylidene fluoride (PVDF) is a highly nonreactive thermoplastic fluoropolymer [2]. It has ferroelectric and piezoelectric properties. It functions better as a receiver than as a transmitter [35]. PVDF has a high optical transmittance, more than 80% between 250 nm and 900 nm. The acoustic impedance is low and it has a wide-band acoustic response. In this way matching and backing layers are unnecessary. Due to the mechanic flexibility of PVDF it can be laminated on a lens [18]. The acoustic impedance of PVDF was 3.89 MRayl [20]. The PVDF that is used has a thickness of 48 μm [36]. The speed of sound is $2.25 \cdot 10^3$ m/s and the acoustic impedance is 3.3075 MRayl [37]. PVDF is resistant for acids and can withstand UV light [38] [39].

The piezoelectric properties of PVDF could be effected by temperature. According to the manufacturer, it could lose around 10% of its performance when heated to 85 degree Celcius. With the comment that a few minutes may not have much effect.

2.5 ITO

The piezoelectric layer should be coated with electrodes to receive the electrical signals [2]. Tin oxide (ITO) is often used as a transparent electrode. The optical transmittance is higher than 60 % for 450 till 1100 nm. However, the conductivity is still limited especially for high-frequency applications. ITO could increase the signal loss and lower the bandwidth of the transducer. So the area of ITO should be minimized. If there is a non-transparent region, that region can be covered with highly conductive metal electrodes to reduce the resistance [18].

The thickness of the coating from the film that is used in this research is less than 30 nm, according to the manufacturer.

2.6 Frequency Response

The center frequency of the transducer is the first resonance frequency of the transducer [40]. The resonance frequency will occur when the transducer is half a wavelength. c = speed of sound, f = frequency, t = thickness, λ = the wavelength.

$$c = f * \lambda \quad (2.5)$$

$$t = \frac{\lambda}{2} \quad (2.6)$$

This gives:

$$f = \frac{c}{2t} \quad (2.7)$$

$$t = \frac{c}{2f} \quad (2.8)$$

$$c_{PMMA} = 2757 \text{ m/s}$$

$$f_{PVDF} = 2.1 \text{ MHz (from FFT)}$$

$$\text{Pulse duration} = 0.001 \text{ ms}$$

$$t = 6.546428571 * 10^{-4} \text{ m} = 0.656 \text{ mm}$$

$$\text{Distance between pulses in PMMA} = 2757 * (0.001 * 10^{-6}) = 2.757 \cdot 10^{-3} \text{ mm.}$$

$$\text{So total thickness, } t_{total} = 0.656 + 2 \cdot 2.757 \cdot 10^{-3} = 0.661 \text{ mm}$$

2.7 Dimensions Transducer

The thickness of the transducer should be at least 0.66 mm to prevent the signals from overlapping. A larger thickness delays the internal reflections more, so a larger thickness will be chosen of 10 mm. The shape will be a square with dimensions of 50x50x10 mm. Also a shape with an angle could be made like described in Section 2.2.2. However, it will be uncertain if that will work, because the PMMA will have to be cut into the desired angle so the cutting-surface will be rough, resulting in scattering.

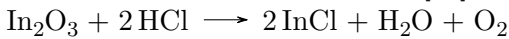
The thickness of the ITO electrodes will be 5 mm, this is quite large, but since the goal is mainly to investigate the cross-talk between the active sides, it would be better to have bigger active sides. In this way, the acoustic waves could be focused more precise on these active sides. The ends of the electrode should be curved, sharp corners could result in voltage spikes and reflections inside the electrode [19].

Chapter 3 Selectively removing ITO

In this chapter the procedure of selectively removing ITO will be investigated. At the end, the final procedure will be described in detail.

3.1 Removing ITO

ITO can be dissolved using HCl [41]. The chemical reaction for that is given by:



The etching rate depends on the concentration of the solvent, as seen in Figure 3.1, and the temperature of the solvent, as seen in Figure 3.2. According to the research of Huang et al. 9M HCl at room temperature is suitable for removing ITO selectively from the glass plate [41].

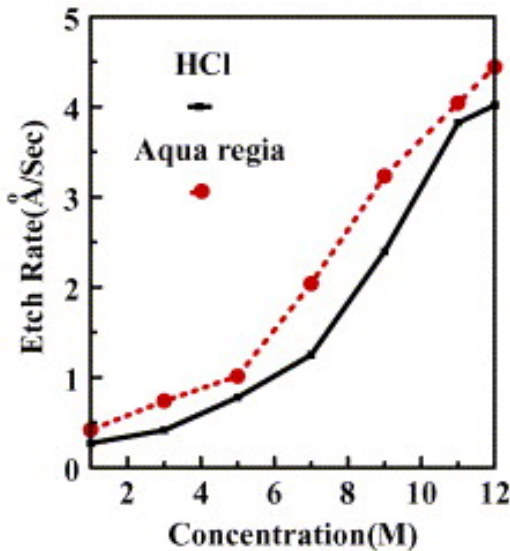


Figure 3.1: Effect concentration of solvent on etching rate at room temperature [41].

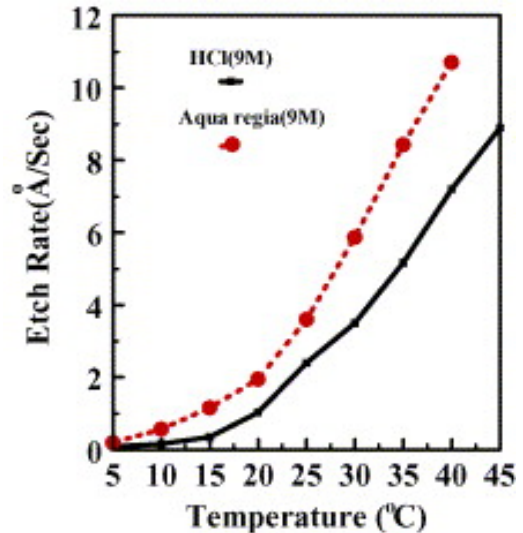


Figure 3.2: Effect temperature of solvent on etching rate both solutions had a concentration of 9M [41].

Choi et al. came to the conclusion that the etching rate of ITO increases under more acidic solvents [42]. First they cleaned the film with 1% sodium dodecyl sulfate solution then rinsed it with deionized water and then rinsed it with ethanol. Right before the experiment, they dried it with nitrogen air and treated it with oxygen plasma for 1 minute.

The thickness of the ITO coating of the PVDF film that is going to be used in the research is approximately 30 nm. If a 9M HCl solution at room temperature is used, the etching rate is 2 Å (follows from Figure 3.1), the time it will take to remove the ITO will be $30/0.2 = 150$ seconds in theory.

Mammana et al. determined the etching rate of various solutions, including 3.2 M HCl. They measured how the resistance developed over time. First they cleaned the film for 15 minutes in a solution (5% Extran®MA02), then rinsed it with deionized water and ethanol. Then put it into the 3.2 M HCl solution. When removing the film from the solution they first put it in water for 1 minute and then rinsed it with ethanol and let it dry. The initial cleaning made the etching faster [43]. In Figure 3.3 the process of solving ITO is visible.

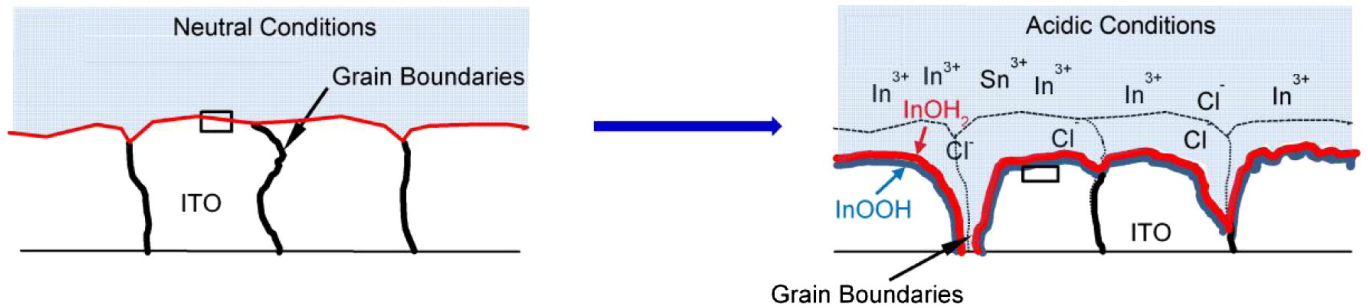


Figure 3.3: Solving process of ITO on thin film [42].

3.2 Etching time

In order to find out the time it takes for the ITO to come off, the following experiment was performed.

3.2.1 Materials

- Fume hood
- 10 pieces of film 5x5 mm
- 5 pieces of film 10x10 mm
- 1% HCl
- 14.5%, 4M HCl
- Ethanol
- Deionized water
- 1% Sodium Dodecyl Sulfate
- Timer
- Low glass work
- Tweezers

3.2.2 Method

10 little pieces of film were cut of approximately 5x5 mm. Then a stock solution was made with a concentration of 14.5% HCl. From that stock solution 1% HCl was made. The films were cleaned by putting them in the 1% sodium dodecyl sulfate for 3 minutes. Afterwards they were placed in water and then in ethanol. Then they dried. This process of cleaning will make the ITO layer be removed faster and at the same rate on every part of the film [42].

When the film was dry again, the pieces were put into the HCl, all at approximately the same time. The ten pieces of 5x5 mm were placed in the 1% HCl solution, every twenty minutes one of the pieces was taken out. The 10x10 mm pieces were placed in the 14.5% HCl solution, every hour one piece was taken out. When a piece was taken out of the solution, it was shortly put in water and then ethanol. Then it dried. When dry, the conductivity was measured to investigate if the ITO was successfully removed.

The same method as described above was used again but then 4 5x5 mm pieces were placed in 1% HCl solution and taken out at 1 minutes, 2 minutes, 5 minutes and 10 minutes.

3.2.3 Results and discussion

In the first 5x5 mm film, that was removed after 20 minutes in 1% HCl solution, no conductivity was measured, which indicates that ITO was removed. There is also a difference in transparency visible. The ITO coating gives the film is a darker appearance than when it was removed (Figure 3.4). No conductivity was measured in the other pieces either. The results indicate that the time for ITO removal in a 1% HCl solution is much faster than was expected. After 1 minute, there was no conductivity measured.

To conclusion; The ITO coating from PVDF could be removed by 1% HCl in 1 minute. Maybe it was better to rinse the films (with water and ethanol), but it was not possible to hold the film because the

tweezers would cover the surface for the most part. The films were really small and therefore difficult to grasp, this grasping may have caused damage to the film.

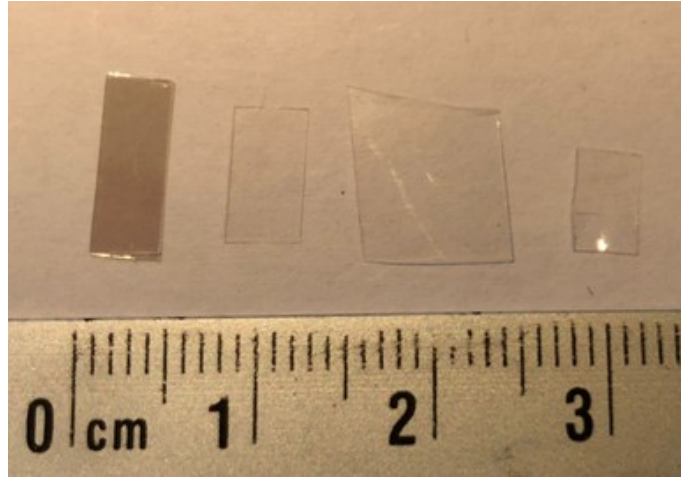


Figure 3.4: PVDF film with different exposure times to 1% HCl. From left to right; 0 min, 20 min, 1 min, 2 min.

3.3 Photoresist Dry Film

Photoresist Dry Film (PDF) is a film that protects the ITO coating from HCl. The PDF can be applied on the PVDF film in the desired shape of the ITO electrodes. The PDF cures under the influence of UV light. The photo initiators inside the dry film absorb the UV light and generate a free radical. This free radical will start a polymerization process. The monomers inside the dry film connect and polymerize further as they also cross-link to each other which makes the structure even stronger. This makes the adhesion between the films strong and therefore the ITO underneath the PDF is preserved [44]. Tsai et al. used a 400 W UV-source for 5 minutes [45].

UV light can cause damage to PVDF when it is exposed for a long time. When this time was less than 40 hours that effect was minimal [46]. So the UV exposure needed for attachment of the dry film should be fine. It could be useful to store the film, and finally the transducers, in a place where it is protected from direct sunlight.

Normally, the PDF is laminated onto the material with heat. However, this is inconvenient for PVDF film, because the film will shrink at high temperature. So in the experiments it is investigated whether PDF also adheres well without adding heat. The melting temperature for PVDF is between 158 and 200 degree Celsius [47], but the piezoelectrical properties could be affected much earlier. According to the manufacturer, the film can shrink in length and lose up to 10% of its performance when heated 85 degree Celsius.

At last, the dry film should be removed from the ITO electrodes. This can be done with sodium hydroxide 5% [44]. However NaOH reacts with PVDF and can cause damage to the PVDF. High concentrations of NaOH react strongly, but it happens with low concentrations too [48]. KOH can also be used to remove dry film. In high concentrations this also reacts with PVDF, but with low concentrations KOH hardly reacts with PVDF [47].

3.3.1 Applying the Photoresist dry film (PDF)

In a dark room a ribbon of the PDF with a thickness of approximately 5 mm was cut. The first protection layer was removed, then the pieces PDVDF were placed onto the ribbon. Then the pieces were placed inside the UV-light source for 5 minutes. After the exposure, the second protection layer was removed. Then the pieces were cut loose by pressing on the connections with the knife. The PDF was hardened, seen by the color change, but fell off very easily. So the procedure was done again, but then the UV-source was heated, 50 and 80 degrees Celsius. In Figure 3.5a, the pieces attached to the PDF are shown. In Figure 3.5b it is clearly seen that the PDF is not attached well and in Figure 3.5c the pieces cleared at 50 degree Celsius are

ready for ITO removal.

As a UV light source, the Formlabs Form Cure is used. Originally, this is a chamber where 3D printed objects could be hardened. It could be heated till 80 degree Celsius and has 13 LEDs with a wavelength of 405 nm [49].

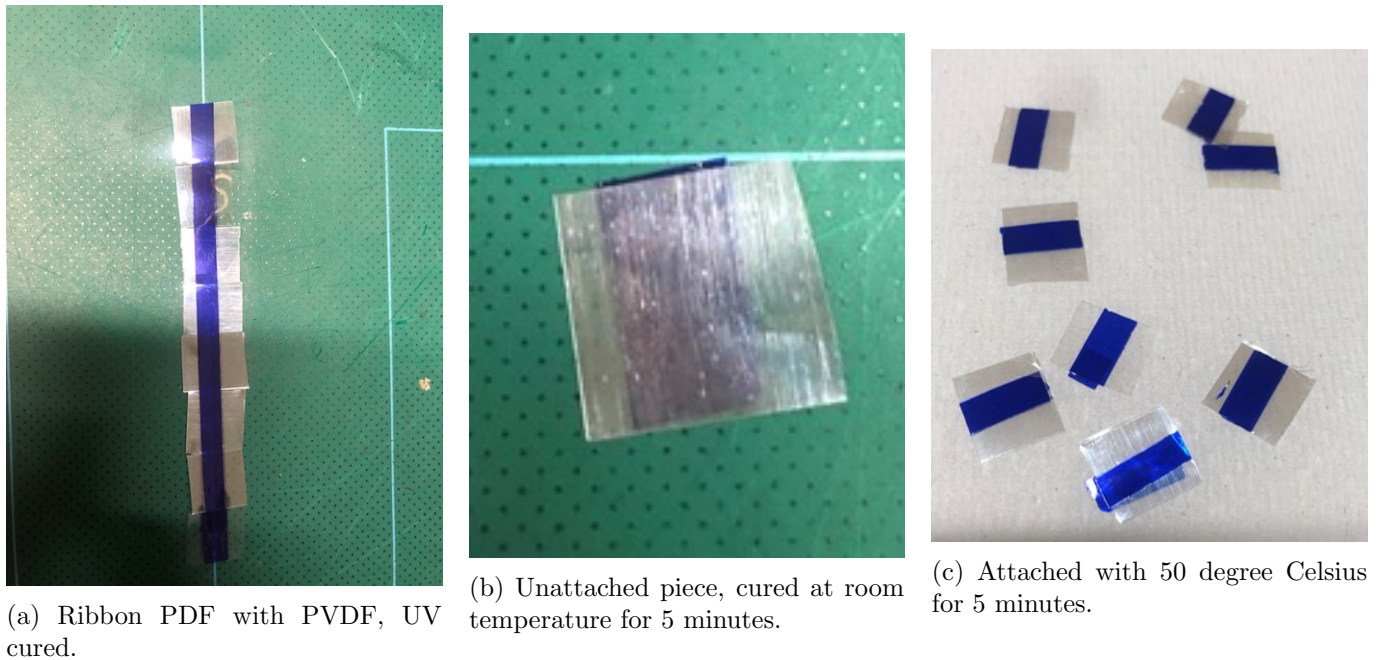


Figure 3.5: Attachment of PDF to PVDF film.

3.4 Removing PDF

Six pieces with PDF cured for 5 minutes at 50 and 80 degrees Celsius were used. First, ITO was removed, using the same procedure as mentioned in Section 3.2. The pieces of film were placed in 1% HCl for 1 minute. After the ITO was removed, this was checked by measuring the conductivity. It turned out that 1 minute was only enough for half the films. So the films were placed in the HCl for a minute more. There was no conductivity measured, so the ITO was removed. The PDF was still intact, in order to remove this, NaOH and KOH were used in different concentrations.

3.4.1 Materials

- 6 PVDF film with dry film and ITO coating removed on the other places type A (cured at 50 degrees Celsius)
- 6 PVDF film with dry film and ITO coating removed on the other places type B (cured at 80 degrees Celsius)
- 5%, 1% and 0.1% NaOH
- 5%, 1% and 0.1% KOH
- Timer
- Deionized water
- Ethanol

3.4.2 Method

First type A film was placed in 0.1% NaOH and 0.1% KOH one minute apart. Then type B was placed in 0.1% NaOH and 0.1% KOH. The time it took the PDF to come off was measured. The film was grasped a few times and shaken inside the solution.

After the PDF was removed, the film was washed in water and ethanol, and then it dried.

This procedure was repeated for the concentrations 1% and 5%.

3.4.3 Results and discussion

The conductivity of the remaining ITO was measured and is shown in Table 3.1 and Table 3.2. It was difficult to measure the conductivity of the ITO layer, since the surface was easily scratched by the multimeter. So the values were unreliable, however, it can be concluded that there was a resistance and that also proves that the ITO has not been removed in that area.

In Table 3.1 it appears that it took 17 minutes to remove the PDF, however the film was pulled off with tweezers. This was not possible with the same concentration with type B, so maybe the film was not attached very well. The ITO shape has much cleaner edges at 80 degrees, see Figure 3.6. For some type B pieces, it took the PDF too long to fall off in KOH, so the time it took could not be noted down, these are referred to as 'n' in the Tables.

Solution	Time (min.sec)	Conductivity (Ω)
5% NaOH	3.20	4.7 M
5% KOH	4.23	31k
1% NaOH	36.00	41 k
1% KOH	70.00	21K, 3.5 M
0.1% NaOH	17.00	6.4 M
0.1% KOH	17.00	3.1k

Table 3.1: Film Type A: cleared at 50 degree for 5 minutes, PDF removed at various concentrations.

Solution	Time (min.sec)	Conductivity
5% NaOH	3.40	45 k, 2.4 M
5% KOH	5.20	n
1% NaOH	16.20	20K
1% KOH	n	n
0.1% NaOH	n	1.2M
0.1% KOH	n	n

Table 3.2: Film Type B: cleared at 80 degree for 5 minutes, PDF removed at various concentrations.



Figure 3.6: Etched films, PDF was removed with several concentrations NaOH and KOH. Color-coded films; red is type A, black is type B. 1 dot is 5%, 2 dots is 1% and 3 dots is 0.1% concentration. The ITO shape in the middle of the films is visible.

The Type A, PDF removed with 5% NaOH was investigated with Optical Coherence Tomography (OCT) to see whether the ITO layer was fully removed from the film. This was indeed the case, see Figure 3.7 and 3.8.

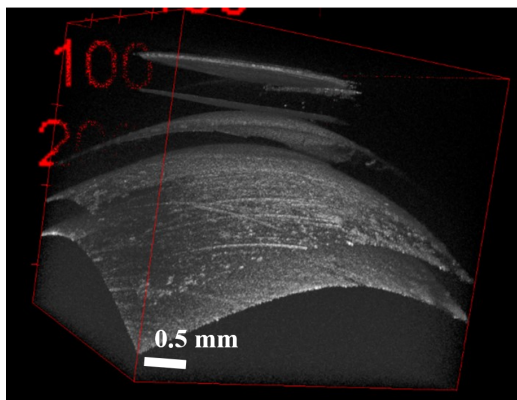


Figure 3.7: Side view, 3D OCT image of the edge of the investigated piece.

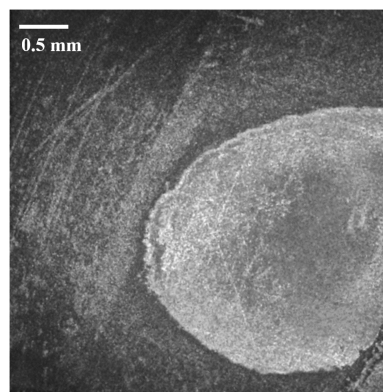


Figure 3.8: Top view, edges of the ITO layer at the top.

There were some remaining questions with the attachment of the PDF. First, it was unclear how high the clearing temperature should be and how long the film should be exposed. Therefore, 6 pieces were investigated once more. They were heated and exposed to UV-light at 60 degree or 80 degrees, for 1, 2 or 5 minutes. Secondly, there were issues with air-bubbles in between the films. This caused etching of ITO at unwanted places. At last, the film should be cleaned before putting on the dry film. This was not done in the previous experiment.

In order to take these factors into account another experiment is performed. First, the film was cleaned. The same way as mentioned before in Section 3.2. Then drops of water were put onto the film. After the first protection layer was removed, the PDF was pressed onto the film with water. This prevented air-bubbles. The films were firmly pressed on each other. This was repeated for the other side. Then they were placed in the heated UV source at 60 or 80 degrees Celsius for 1, 2 or 5 minutes. When bending the film, the PDF came off at the 60 degree Celsius pieces and also at the 1 minute 80 degree Celsius piece, see Figure 3.9. The 2 minute 80 degree Celsius film was a bit loose at the corners. The 5 minute 80 degree Celsius pieces attached quite well and should give a good ITO layer with sharp edges. In Figure 3.10 the piece that was heated at 80 degrees Celsius and exposed for 5 minutes is seen when ITO was selectively removed. The edges are quite sharp.

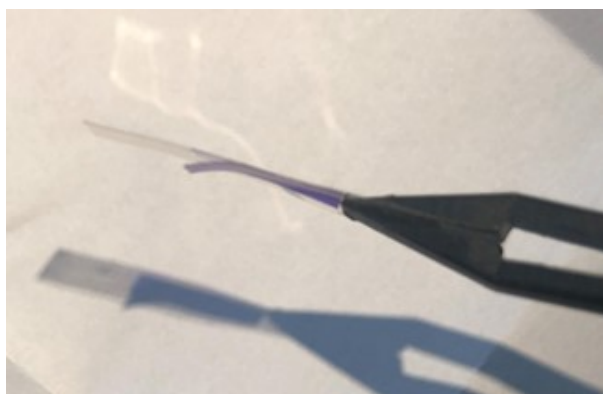


Figure 3.9: The PDF came off the 60 degree films, quite easily when bending the film



Figure 3.10: Etched piece, heated at 80 degrees exposed to UV light for 5 minutes.

It was quite difficult to determine the right solution for the removal of PDF. Because the film can be damaged by using the removal solutions, but it cannot be seen how much. So initially, 1% NaOH for approximately 30 minutes will be used to remove the PDF.

3.5 Final Procedure

In order to conclude this chapter, the final procedure is described.

3.5.1 Material

- PVDF film
- Photoresist dry film (PDF)
- Formlabs From Cure (UV source)
- 1% HCl
- Deionized water
- Ethanol
- 1% Sodium Dodecyl Sulfate (SDS)
- 1% NaOH
- Tweezers
- Timer
- Fume hood
- Low glass work

3.5.2 Method

1. Clean the film, by putting the film inside 1% SDS for 3 minutes. Then rinse the film with deionized water and then rinse with ethanol. Let the film dry.
2. Cut the photo resist dry film (PDF) to the desired shape, Figure 3.11. This has to happen with minimum exposure to UV light. But for short periods of time it is acceptable to have daylight.
3. Spray deionized water onto the film. Then remove the first protection layer of PDF and press the PDF onto the PVDF film. Repeat this for the other side, see Figure 3.12a. Place the film between something like a book or cover it with aluminum foil to protect it from UV light.
4. Heat the UV-source to 80 degrees Celsius, place the film inside for 5 minutes. Remove the second protection layer, see Figure 3.12b.
5. Clean the film again like mentioned in step 1.
6. When it is dry, place it in the HCl solution for 2 minutes. When taking the film out, rinse with water and ethanol and let dry, see Figure 3.12c.
7. Place the film in 1% NaOH for approximately 30 minutes and let the PDF fall off. Then rinse the film with water and ethanol, see Figure 3.12d.

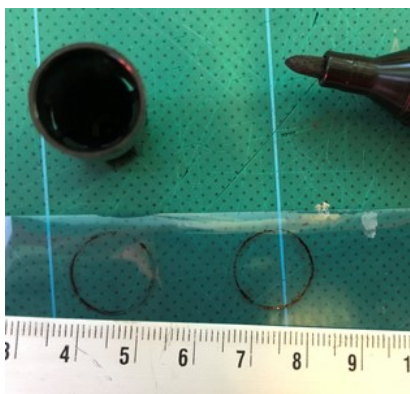


Figure 3.11: Marking the PDF using the lit of the marker.



(a) PVDF with ITO coating and uncured PDF.



(b) PVDF with ITO coating and cured PDF, 80 degrees Celsius, 5 minutes in UV source.



(c) PVDF with ITO coating removed.



(d) PVDF with ITO circle and PDF removed.

Figure 3.12: Process of selectively removing ITO.

Chapter 4 Making the Transducer

In order to construct the transducer several steps are taken. First the PVDF film is prepared by selectively removing ITO, then the PVDF film is glued onto the substrate and at last the connection of the film to the oscilloscope is made.

4.1 Materials

- Photoresist dry film
- 5 mm washer
- Permanent marker
- Scissors and surgical knife
- Distilled water
- Substrate; PMMA 65x65x8 mm
- PVDF with ITO coating 55x55 mm
- Conductive epoxy, circuit works CW2400
- 4 copper wires
- Epoxy, NOA85V
- Formlabs From Cure (UV source)
- Soldering iron
- Tin
- Cable

4.2 Method

4.2.1 PVDF film

First the PVDF film with the electrodes was made, as described in Section 3.5. Four ribbons of PDF were cut with a width of 5 mm. The curve at the top was marked using a 5 mm washer and then this curve was cut from the ribbon with scissors. Two ribbons were placed on the top and two on the bottom side of the film. The film had dimensions of 55x55 mm. To get the distance between the active regions right, the film was taped onto a template in the lab journal, see Figure 4.1. After the ITO was selectively removed, conductive epoxy was used to attach copper wires to the ITO coating ends. This conductive glue had to dry for a few hours before the rest of the transducer could be made.

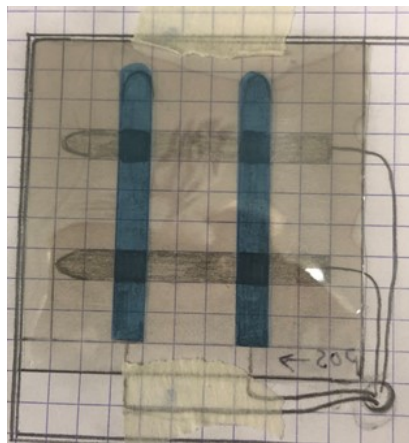


Figure 4.1: PVDF film taped on the electrode template.

4.2.2 Substrate and attachment

The substrate was PMMA with dimensions of 65x65x8 mm. The epoxy (NOA85V) was applied on the substrate with a disposable pipette. The glue should cover the whole substrate except 10 mm from the two sides from the opposite corner of where the film is placed. The viscosity of the epoxy was very low, this caused the epoxy to escape from under the PVDF film when the PVDF film is pressed onto the substrate. In order to overcome this the substrate with the epoxy is placed in the UV chamber for 1 minute. Then the epoxy was more viscous and the film could gently pressed onto the substrate. The film should be attached with the positive side up. The regions where the copper wires were attached at the bottom with conductive epoxy were not glued onto the substrate to get the film straight.

The PVDF film was applied on the substrate in one corner from one side of the film and then slowly let down. This prevented air-bubbles in between. The few air-bubbles that were present were carefully pressed to the sides of the film. Then another PMMA piece with the same size was used to gently press on the film to make sure that the film is flat and pressed onto the substrate equally, see Figure 4.2. Then the substrate was placed into the UV chamber for 5 minutes. This was sufficient for good attachment, see Figure 4.3.

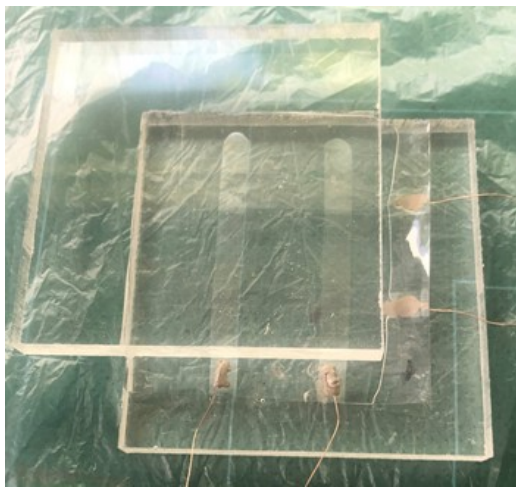


Figure 4.2: Pressing the PVDF film gently on the substrate.

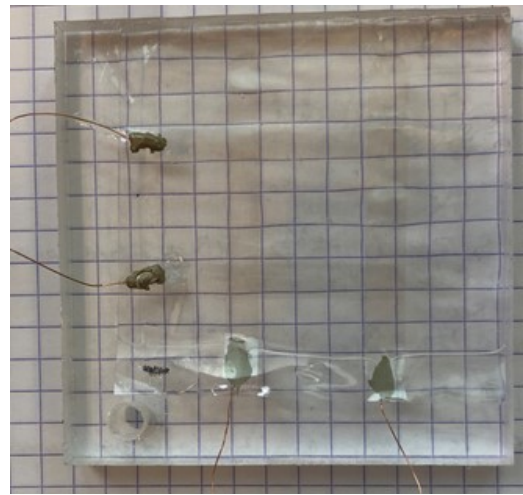


Figure 4.3: Film attached to the substrate.

4.3 Electronics

The copper wires of the film should be attached to the pre-amplifier. To make this possible every copper wire was soldered to another wire. A hole of 5 mm was drilled in the substrate to let the wires go through. Superglue was applied inside the hole. In this way no tension on the film or copper wires is applied from pulling the wire. The wires were screwed into PCB terminal block. These PCB inputs are connected to a print board with copper lines, see Figure 4.4. The lines are connected to a toggle switch, the wires that come from the columns were connected to the same switch, the same holds for the rows. In this way, it is possible to choose a column and row, so the active region of interest can be selected. The current flows in the switch from the chosen side to the middle. So the middle of the switch is connected to the output. The output is a female BNC and can be easily connected to the amplifier. The electronic circuit of the switchbox is drawn in Figure 4.4a.

To house these electronics a 3D printed case is designed, see Figure 4.4c and 4.5. The orientation of the transducer, the way the selection of the active region works and the way the colored wires should be screwed in the case, is written on the case. When another 2x2 array transducer prototype is made, the electronic case could be easily reused. However the color-codes and orientation of this prototype should be taken into account. The transparent transducer with the switch box connected is shown in Figure 4.6.

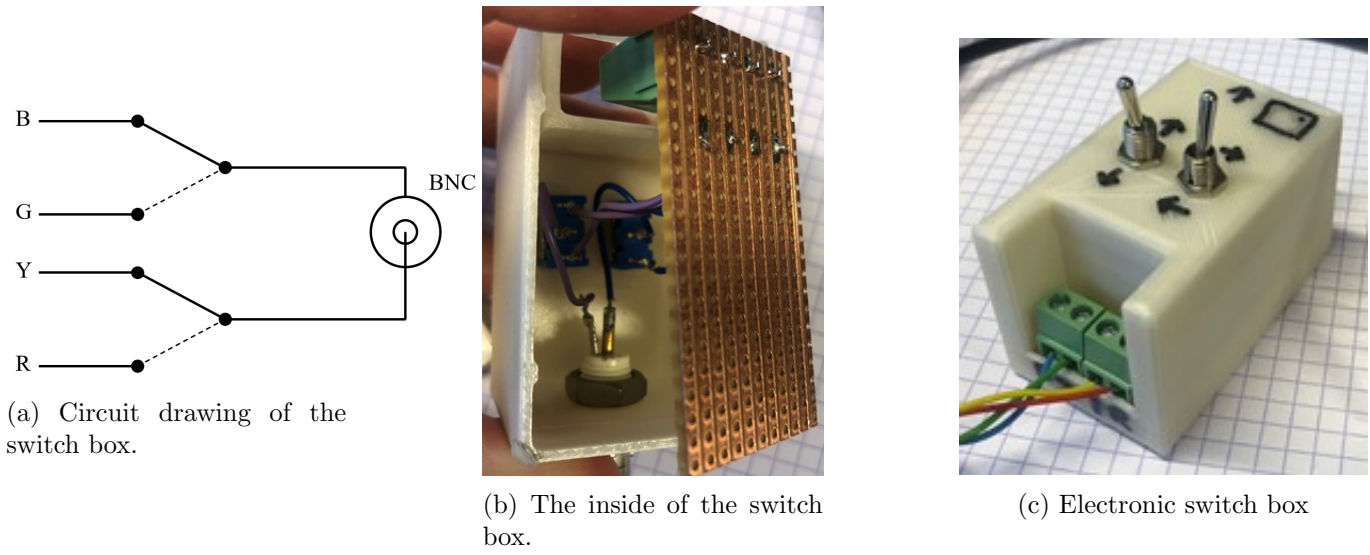


Figure 4.4: The switch box, with the instructions on the top.

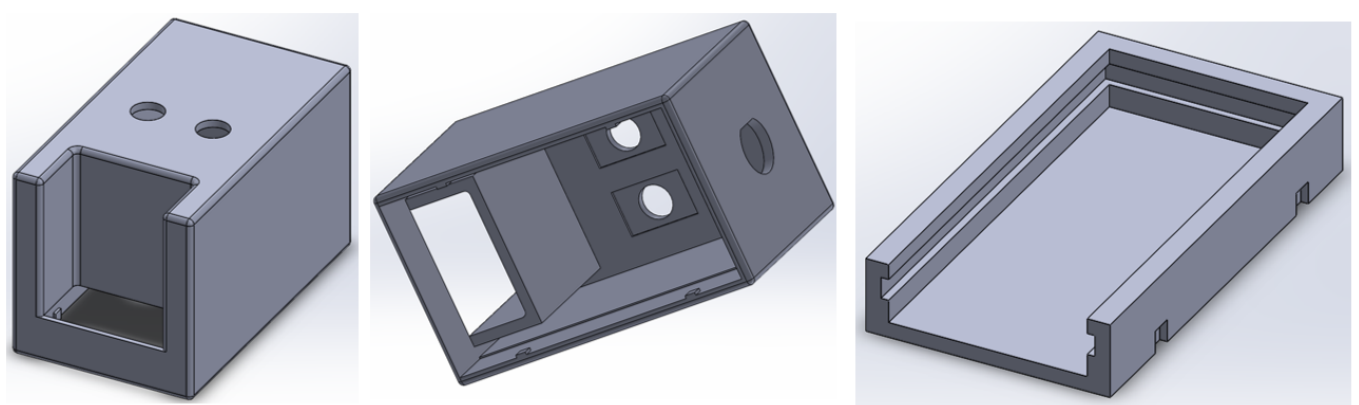


Figure 4.5: Solidworksmodel for 3D printed switch box. Respectively; the lid of the box viewed from the front, viewed from the bottom, the baseplate of the box.

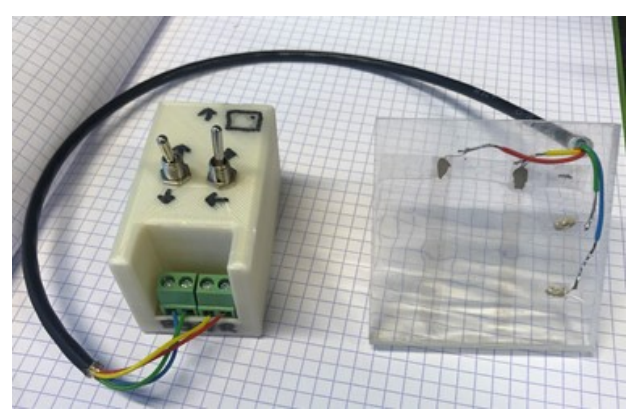


Figure 4.6: The transparent transducer 2x2 array, prototype 1 with switchbox.

Chapter 5 Characterizing and Testing

In this chapter the results of testing the transducer is shown.

5.1 Testing the effect of the process of ITO removal on the performance

The procedure of removal of ITO could damage the film. Heating for 5 minutes at 80 degrees could reduce the performance and washing in NaOH could cause stress cracking [48]. To investigate to what extent the film was damaged after the procedure, a film before the procedure was measured and compared to a film after the procedure.

First, a piece of PVDF film was made with a circle of ITO coating in the center. The diameter of the ITO coating was 15 mm and the ITO coating was on both sides in the same shape. The process of making the film is described in Section 3.5. This film was connected to an SMB cable by gluing copper wires onto the ITO with conductive glue, then these copper wires were connected to the SMB cable by soldering. Heat shrink tubes were used to protect these wires from short-circuiting with each other.

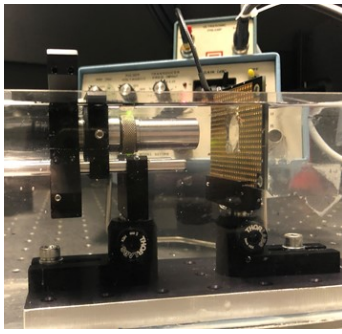
In the setup a focused transducer of 2.25 MHz was used with a focal length of 20 mm. With the Abbe diffraction limit, the radius of the smallest possible focus could be calculated (d). The Abbe diffraction limit is given in equation 5.1. n is the refractive index, this is only relevant in optics, so n = 1. θ is the opening angle of the transducer. D is the diameter of the transducer, D = 15 mm, f is the focal length. For the wavelength equation 5.2 is used, where c is the speed of sound, which is 1480 m/s for water and fr is the frequency.

$$d = \frac{\lambda}{2NA} = \frac{\lambda}{2n\sin(\theta)} \approx \frac{\lambda f}{nD} \quad (5.1)$$

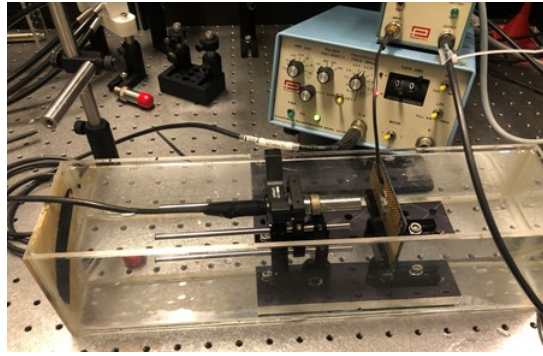
$$\lambda = \frac{c}{f_r} = 658\mu m \quad (5.2)$$

Combining equation 5.1 and 5.2 gives: $d = 877 \mu m$, the radius of the smallest possible focus of the transducer.

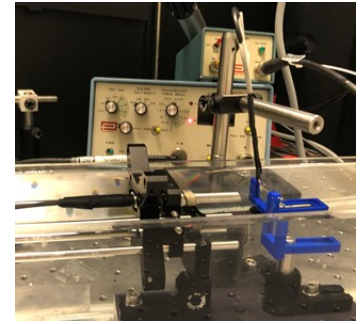
In Figure 5.1a the transducer with the unprocessed film was placed in the setup. This transducer was used in previous work. In Figure 5.1b the complete setup is shown. And in Figure 5.1c the setup with the film is seen. In Figure 5.2 a schematic overview is given. The setup consists of a water basin with distilled water. The 2.25 MHz unfocussed transducer is connected to a pulse receiver (panametrics square-wave pulser/receiver model 5077PR) and gives acoustic waves. This pulse receiver is connected to the oscilloscope (Tektronix TDS 2022B) as external trigger. The transparent transducer is connected to a 40 dB pre-amplifier (panametrics ultrasonic preamp model 5678) and this amplifier is connected to channel 1 (CH1) of the oscilloscope. The data is derived from the oscilloscope with a USB.



(a) The setup with the PVDF film before the procedure.



(b) Overview of the whole setup.



(c) The setup with the film after the procedure.

Figure 5.1: Setup for testing the unprocessed and processed PVDF film.

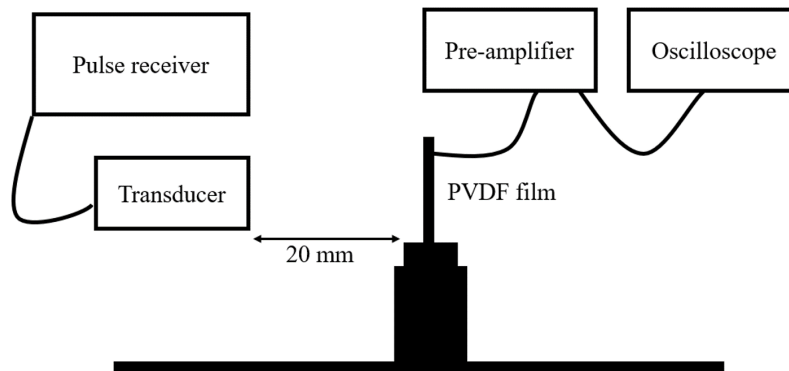


Figure 5.2: A schematic overview of the setup for testing unprocessed and processed PVDF film.

In Figure 5.3 the results of both of the films are shown. These graphs do not match very much. Because the processed PVDF film is not attached to a stiff substrate, the film is wrinkled a bit. This may have caused the PVDF film to move with the sound waves.

To improve the stiffness of the processed PVDF film, the PVDF film is attached to a glass slide with double-sided transparent tape, see Figure 5.4. Then the transducer is placed in the holder. However, when placing the transducer in the holder the glass slide and the film broke. It was not possible to do measurements with it anymore. So a new transducer was made, this transducer had a slightly different design in order to make it easier to connect to the SMB cable, see Figure 5.5. Further on, a transducer is made with the same dimensions but with unprocessed film.

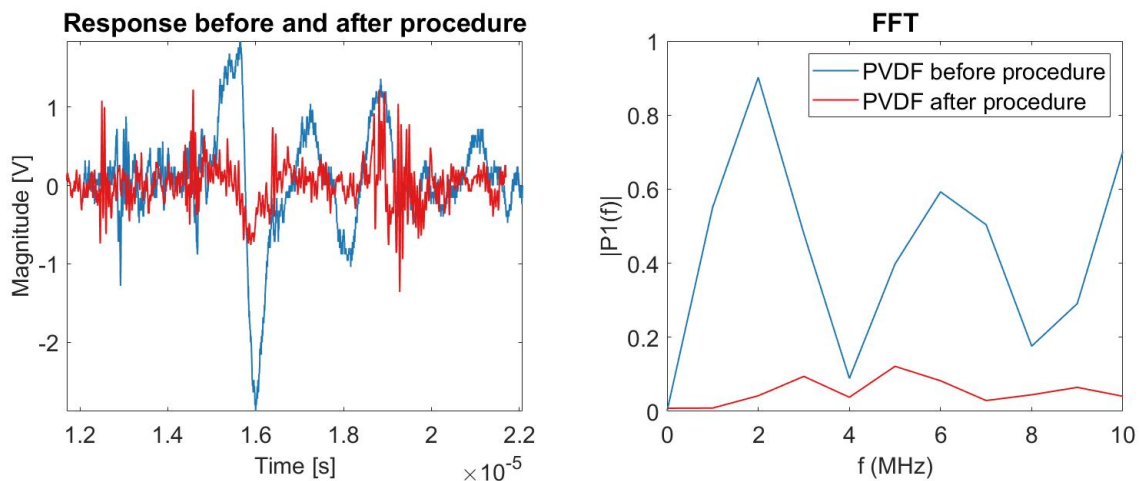


Figure 5.3: Unprocessed film and processed film compared with each other at 2.25 MHz. Left the raw signal and right the frequency response.



Figure 5.4: Transducer with circular ITO coating placed on glass slide



Figure 5.5: The transducers for testing the films properties. Processed film left and unprocessed film right.

The glass slide does not fit entirely into the holder. The distance between the glass slide and the top of the metal base is 12 mm, see Figure 5.7. A setup with a vertically moveable transducer was built, see Figure 5.6. The transducer could be shifted with steps of 0.1 mm.

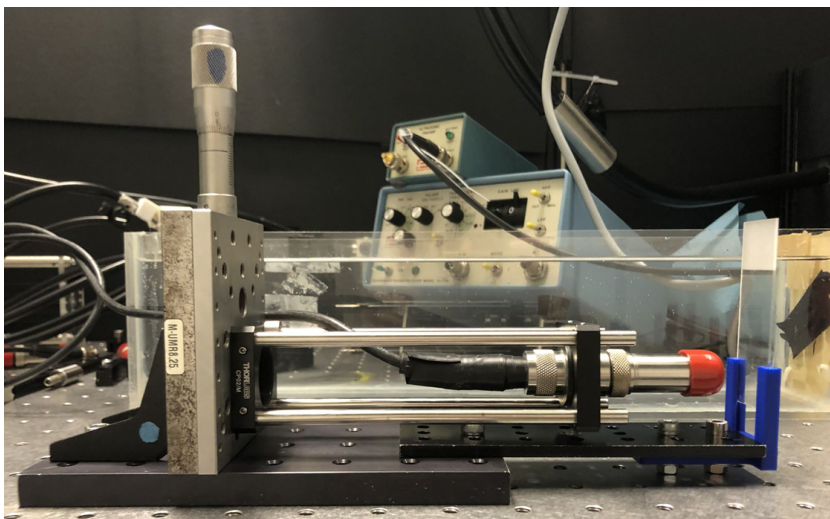


Figure 5.6: he setup with moveable transducer

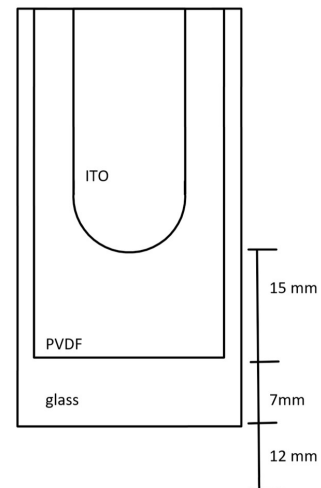


Figure 5.7: Transparent transducer configuration

A 2.25 MHz unfocused transducer was used and placed 20 mm from the transparent transducer. The pulser voltage was 100 and the signal was amplified with a gain of 30 dB. In Figure 5.8 the time series and the frequency responses are shown. The amplitude of the unprocessed film is around 3 times higher, so the performance after the procedure decreases. There is a small shift visible in the time series, but the shape is comparable. The shift could come due to positioning of the transparent transducer, when replacing it the distance between the transducers could change just a little which can cause this shift. The shape of the frequency response is the same for both signals.

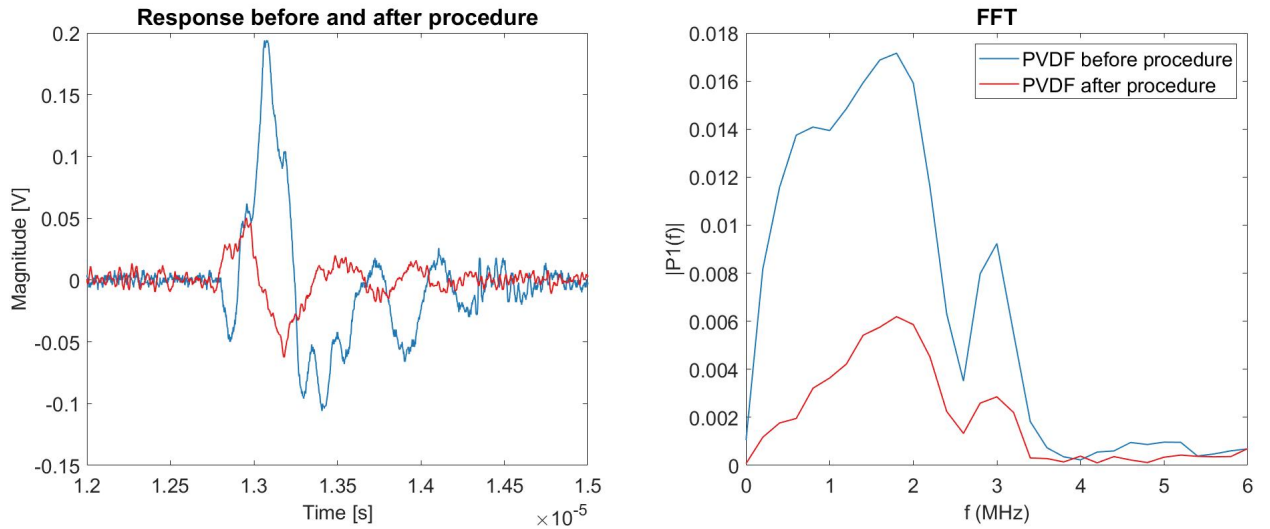
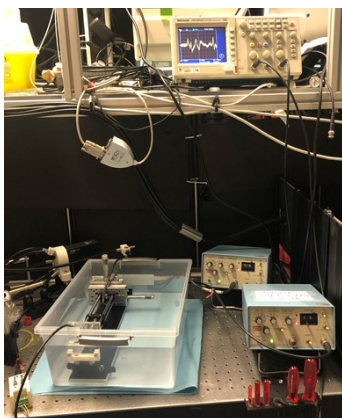


Figure 5.8: Signals of the (un)processed transducers compared. left the time series and right the frequency-response.

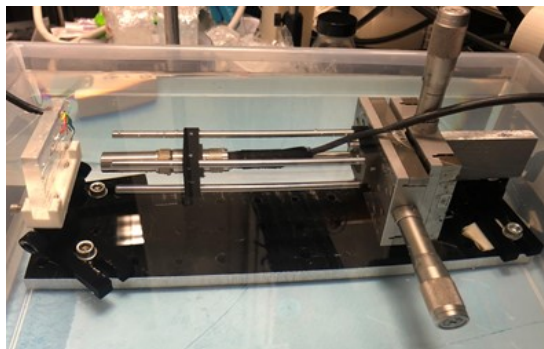
5.2 Testing the transducer

5.2.1 The setup

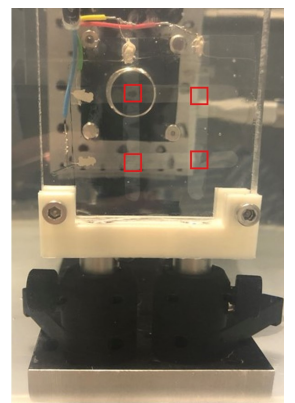
In Figure 5.9 the setup for testing the transducer is shown and in Figure 5.10 the schematic drawing of the setup is shown. There are two movable stages onto each other, which makes it possible to move the transducer in x (horizontal) and y (vertical) direction. In this way it is possible to focus anywhere on the transparent transducer. The stages are placed on 2 postholders, using an aluminum plate that was custom-made for this. The transparent transducer itself is placed in a 3D printed holder that is placed on 2 postholders, see Figure 5.11. The height of the transparent transducer could be easily tuned in this way. The pulse-receiver is connected to the transducer, this transducer transmits acoustic waves onto the transparent transducer. The transparent transducer is connected to the second pulse receiver by the switch box. This second pulse receiver only functions as a pre-amplifier for the received signal. The switch box is connected to the oscilloscope.



(a) Complete setup.



(b) Setup from side.



(c) Setup from the front, with the transducer focusing on an active region. The active regions are marked with red squares.

Figure 5.9: Setup with movable transducer in x and y direction.

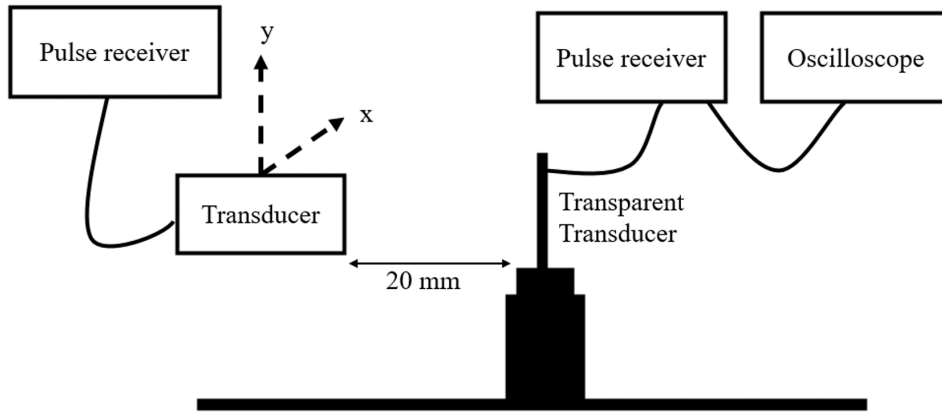


Figure 5.10: Schematic drawing of the setup with moveable transducer in x and y direction.

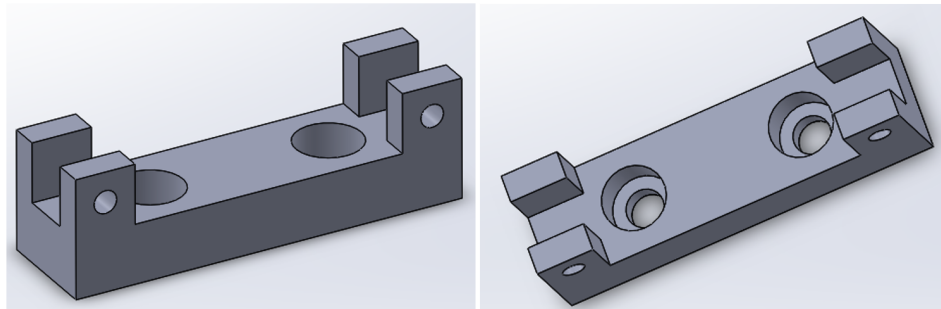


Figure 5.11: Solidworks model of the transducer holder

5.2.2 First test with Prototype 1

Prototype 1 is made according to Section 4, the prototype is shown in Figure 5.12. The active regions where the ITO is overlapping are numbered. When seen in coordinates; region 1 is (1,2), region 2 is (2,2), region 3 is (1,1) and region 4 is (2,1).

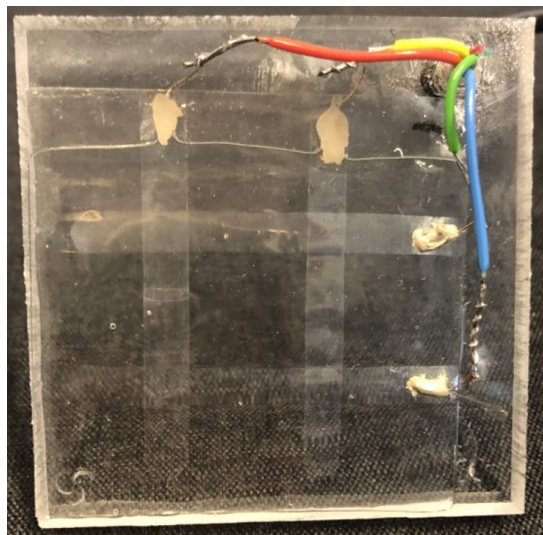


Figure 5.12: Transparent transducer, prototype 1

The movable transducer was aimed at an active side of the transparent transducer. Then the signal of every active side was measured. A focused transducer with a frequency of 2.25 MHz was used, the gain was 30 dB and the pulser voltage was set at 300. The switch box was attached to the pulser receiver, the active region of interest could be manually selected by the switch box.

The time series and frequency response of the signal were plotted in Matlab. The signal is shown in Figure

5.13. The internal reflections are also visible and marked with a red circle. To get a better visualization, a bar graph of the maximum value of the amplitude minus the minimum value of the amplitude was made, see Figure 5.14. This was done by using a peak selection function in Matlab, the maximum value was selected and then the minimum value. These values were subtracted and then plotted into a bar graph.

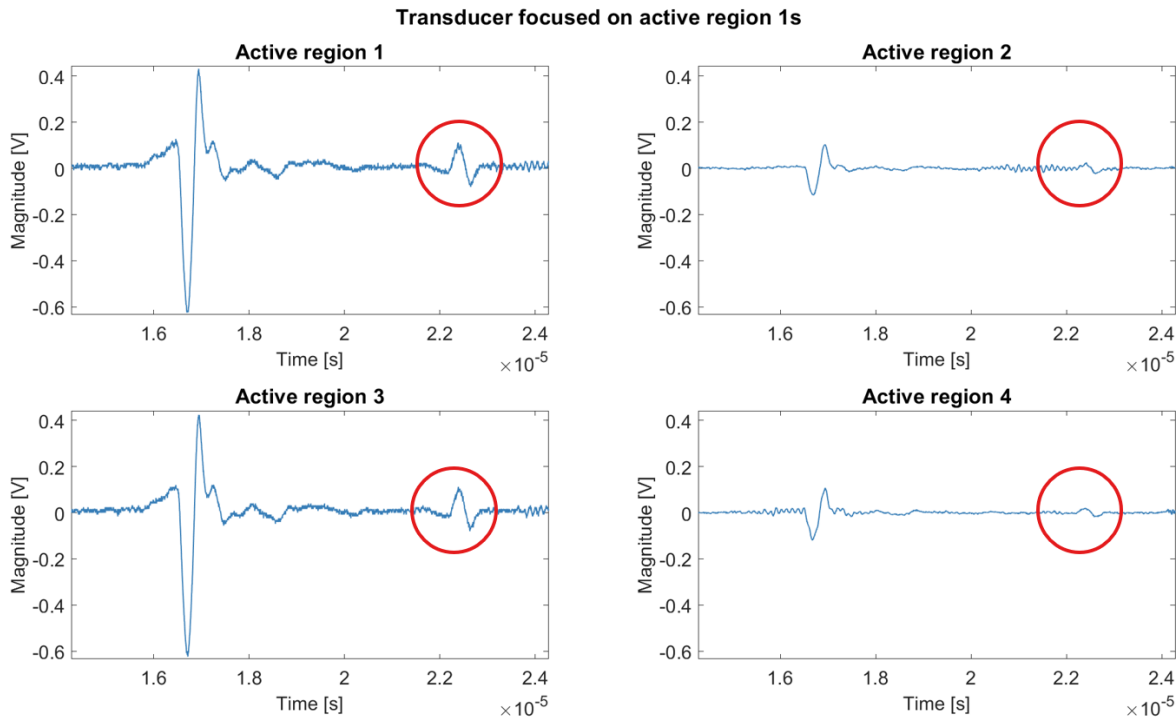


Figure 5.13: The signal of all active regions, when the transducer was focussed on active region 1. The internal reflections are marked with red circles.

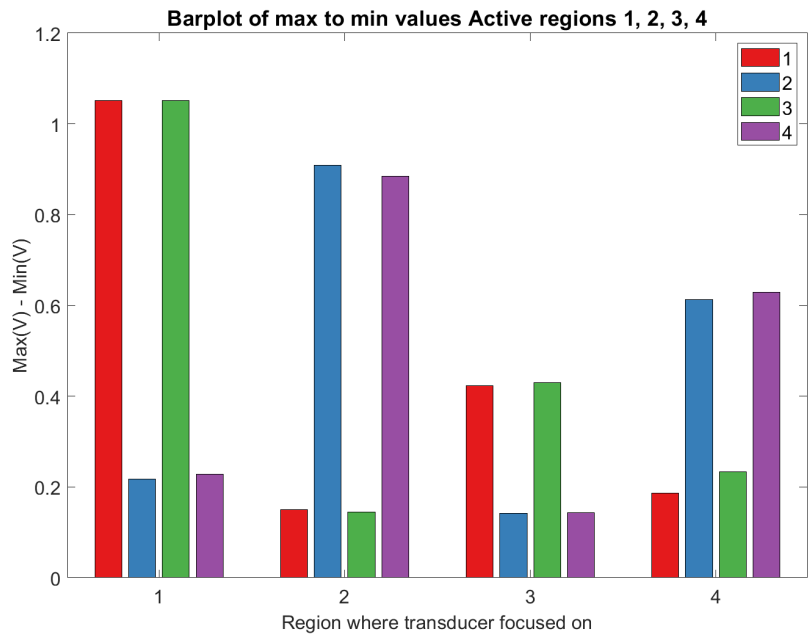


Figure 5.14: Bar graph of maximum - minimum values of the measurements.

What stands out in these figures and the other figures, where the transducer is focused on the other active regions, is that active region 1 and 3 are the same and 2 and 4 are the same. With other words; the columns differ, but the rows do not. Further on, the shape of the graphs are the same, only a higher or lower amplitude.

5.2.3 Focusing on multiple regions

To examine this behavior more, different regions of the transducer are examined. In Figure 5.15 the different regions that the transducer was divided into are visible. The capital letters are placed at regions without ITO, the lowercase letters are at regions with ITO on one side. The numbers are the active regions.

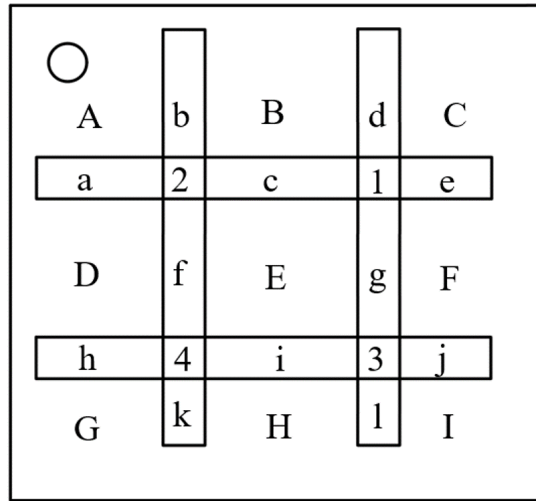


Figure 5.15: The back view from the transducer divided into regions. The capital letter are placed at regions with no ITO, the letters without capital letter are at regions with ITO on one side. The numbers are for the active regions.

The movable transducer was focused onto all regions, the signal of the active sides was measured. In Figure 5.16 the bar graph of regions c, f, g and i is visible. The graphs of f and g are much higher than those from c and i. The film works like a capacitor, which means that there is a line integral. And the ribbon ITO distributes voltage over that line, that is why the graphs of 2 and 4 are the high at f and 1 and 3 are high at g.

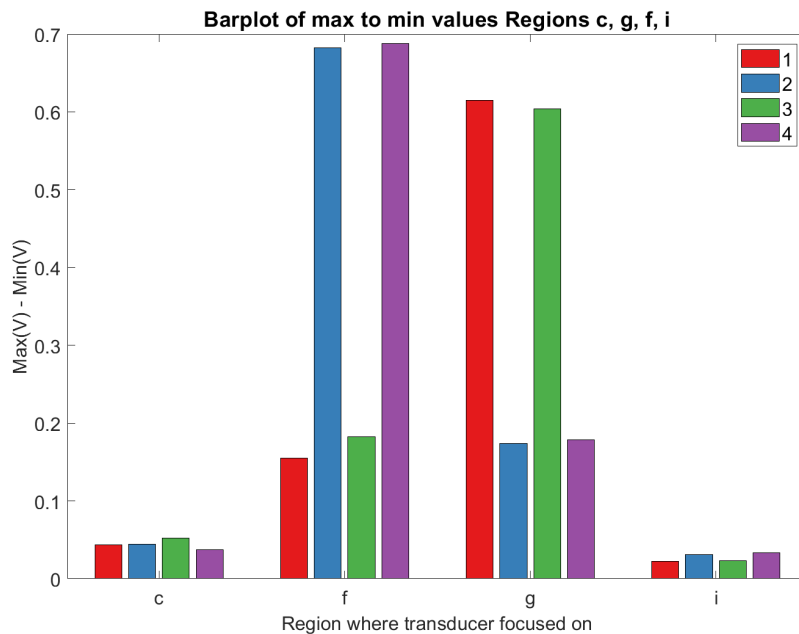


Figure 5.16: The bar graph of regions c, f, g and i.

In Figure 5.17 the bar graph of regions B, D, E, F, H is shown. These signals are all very low compared to when the transducer is focused on the active regions. So these signals could be all considered noise. With other words, if the transducer is focused on a region without ITO this does not transmit to the active regions.

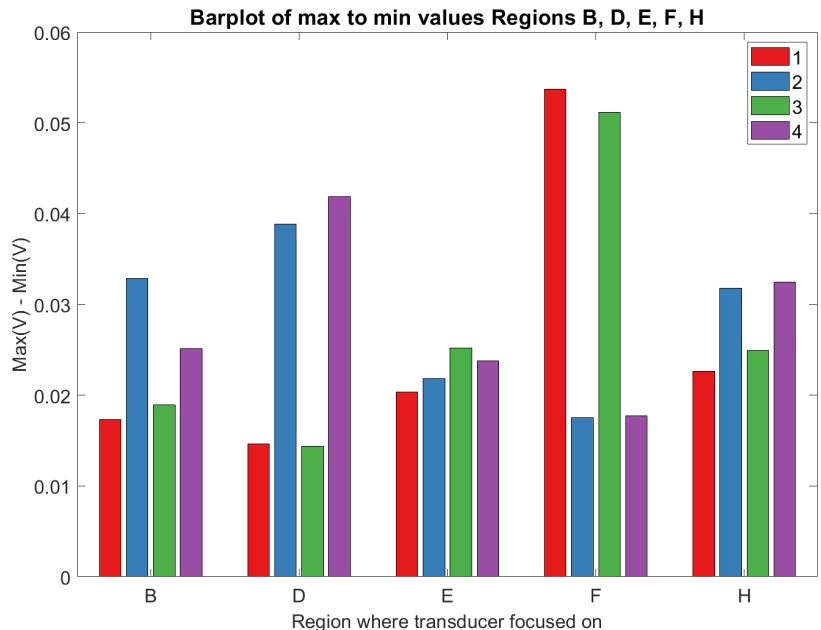


Figure 5.17: The bar graph of regions B, D, E, F, H.

5.2.4 Inverting the transparent transducer 180 degrees

When inverting the transparent transducer 180 degrees the signal stays the same, see Figure 5.18. This means that the columns differ, but the rows do not. So it is not based on where the ITO coating is located, the front or the back of the film/ positive or negative side.

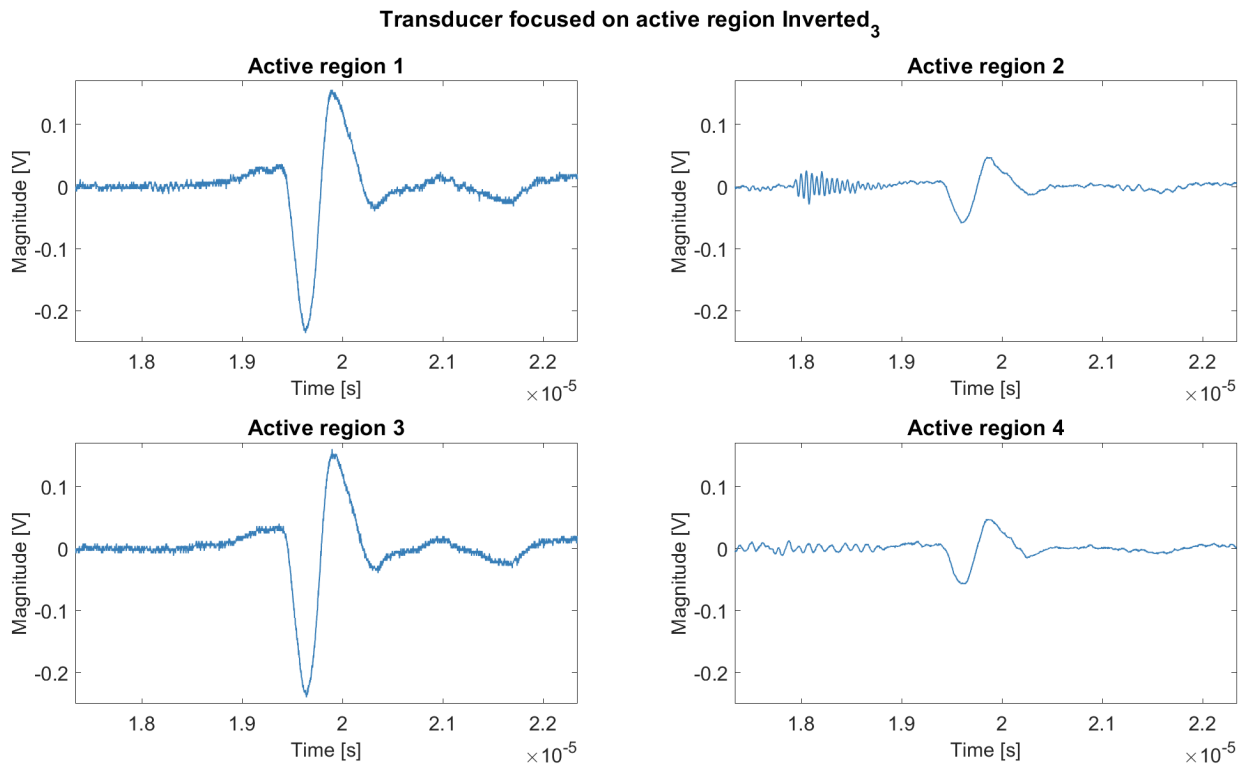


Figure 5.18: The transparent transducer is inverted, and the transducer was focused on active region 3.

5.2.5 Swapping the cables in the switch box

The idea of measuring the active regions is based on the voltage difference over the film. This voltage difference is measured with ITO electrodes at the 4 active regions. Therefore a BNC cable is used. The outer part of the BNC functions as a ground. The middle part of the BNC is the signal with respect to that ground, see Figure 5.19. In the previous measurements, the ground was connected to the row electrodes which are at the positive side (front) of the film. An experiment is performed when this is switched, so the column electrodes at the negative side (back) of the film are now connected to the ground.

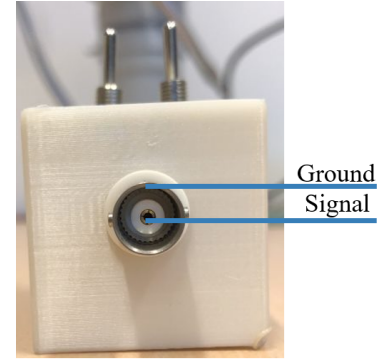


Figure 5.19: BNC output of the switch box.

In Appendix A the results of these measurements are seen. The transducer was focused at region 3, region 1 and 3 still have the same shape, so have 2 and 4. The amplitude slightly changed, see Appendix A. Swapping the column electrodes to the ground did not change the results.

5.2.6 Prototype 2

The results suggested that the ITO of the front part was not removed well. To exclude this hypothesis, a new transducer was made, Prototype 2. This transducer had the same procedure and design of Prototype 1. But then the film was exposed to ITO for 10 minutes instead of 2 minutes. In Figure 5.20 the signal is shown when the transducer is focused on active region 1. The rows don't differ, 1 and 3 are the same and 2 and 4 are the same. This was also the case when focusing the transducer on active region 2. When focusing on active region 3 and 4, only noise is measured. So these measurements were unusable. However it can be concluded based on the measurements when focusing on region 1 and 2 that the same behavior was observed, so the etching of ITO at the front of the film is not the reason that the rows do not differ.

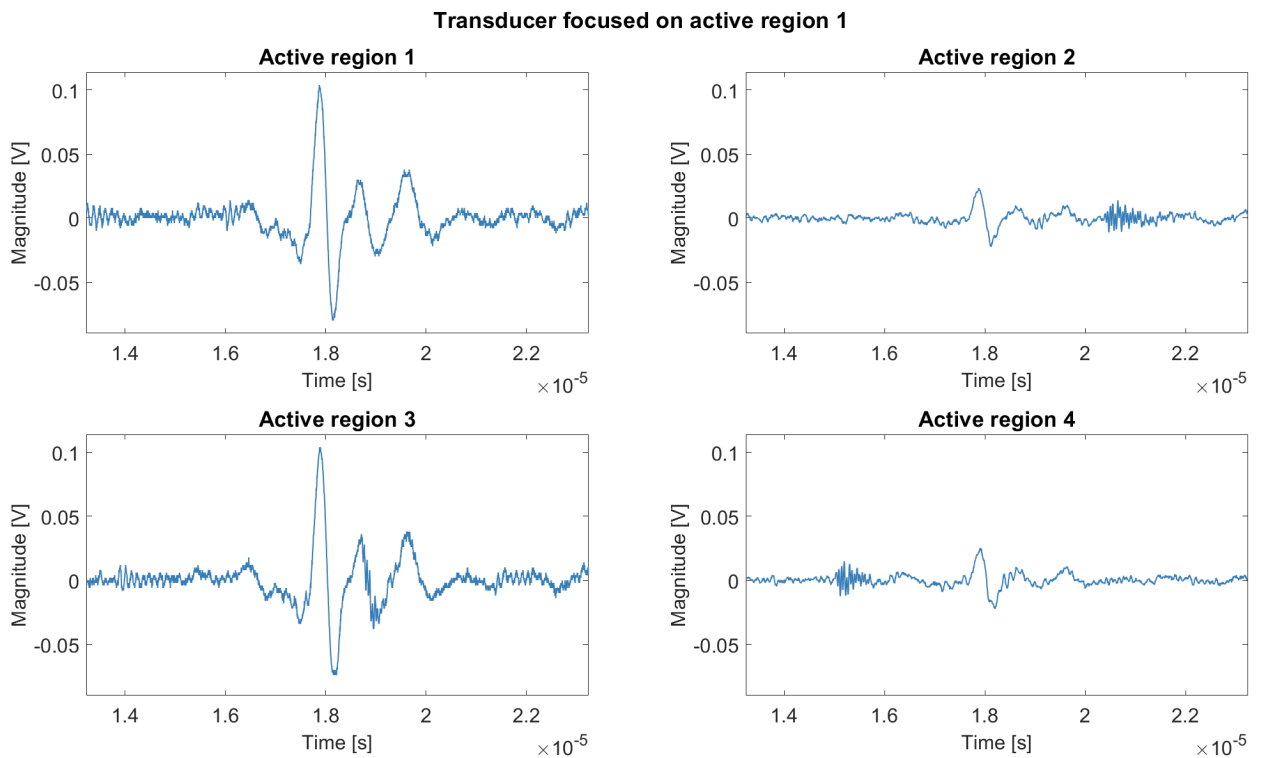


Figure 5.20: Signal from Prototype 2, gain 30 dB, focused on active region 1.

5.2.7 Grounding the transparent transducer to the power supply ground

The columns or rows connected to the outside of the BNC (ground of the BNC) are functioning as floating ground. Meaning that they are not connected to the power supply earth. The oscilloscope is grounded to the power supply earth, so it has a different reference than the ground of the transparent transducer. For accurate testing, it is important that the oscilloscope has the same ground as the transparent transducer [50]. This may be the cause of the problem that the row do not differ.

An experiment is performed to find out more about the behavior of the transparent transducer due to grounding. The transducer (focused 2.25 MHz) was focussed on region 2 marked blue in Figures 5.21 and 5.22. First active region 1 (marked red in Figure 5.21 and 5.22) is measured by connecting the row from 1 to the red alligator clip, this goes to the middle pin of the BNC. The column from 1 goes to the black alligator clip, this goes to the outer part of the BNC. The rest of the wires are clamped to the table, so they are grounded at the power supply ground the same way as the oscilloscope, see Figure 5.21 for a schematic overview of the connections. Region 1 is measured a second time but then the column is connected to the middle of the BNC and the row to the outer part, see Figure 5.22. These measurements are repeated for every active region in the same way.

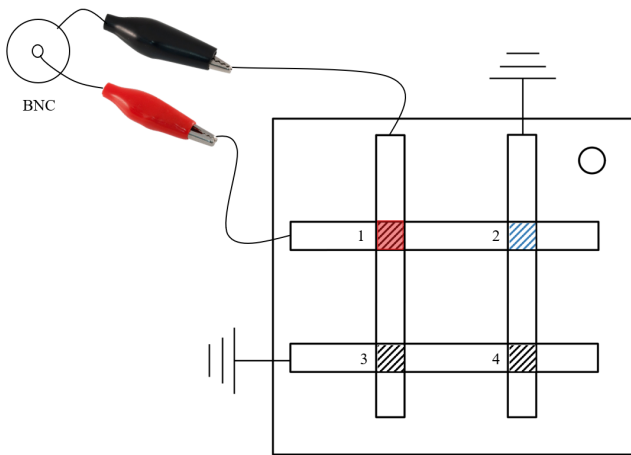


Figure 5.21: Transducer is focussed on region 2, region 1 is measured by connecting the column to middle of the BNC and the row to the outerpart of the BNC.

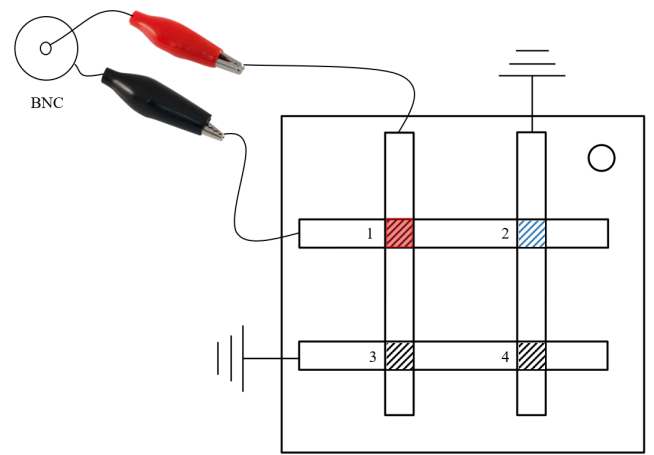


Figure 5.22: Transducer is focussed on region 2, region 1 is measured by connecting the row to middle of the BNC and the column to the outerpart of the BNC.

The results of the first measurements, rows connected to middle and columns to the outer part, can be seen in Figure 5.23. In this case, 1 and 2 are the same and so are 3 and 4. So the rows differ and the columns do not. The results of the second measurements, columns connected to middle and rows to the outer part, can be seen in Figure 5.24. Here, 1 and 3 are the same and 2 and 4 are the same. So the columns differ and the rows do not.

To conclude, when connecting the unmeasured wires to the earth, differentiation in rows could be obtained.

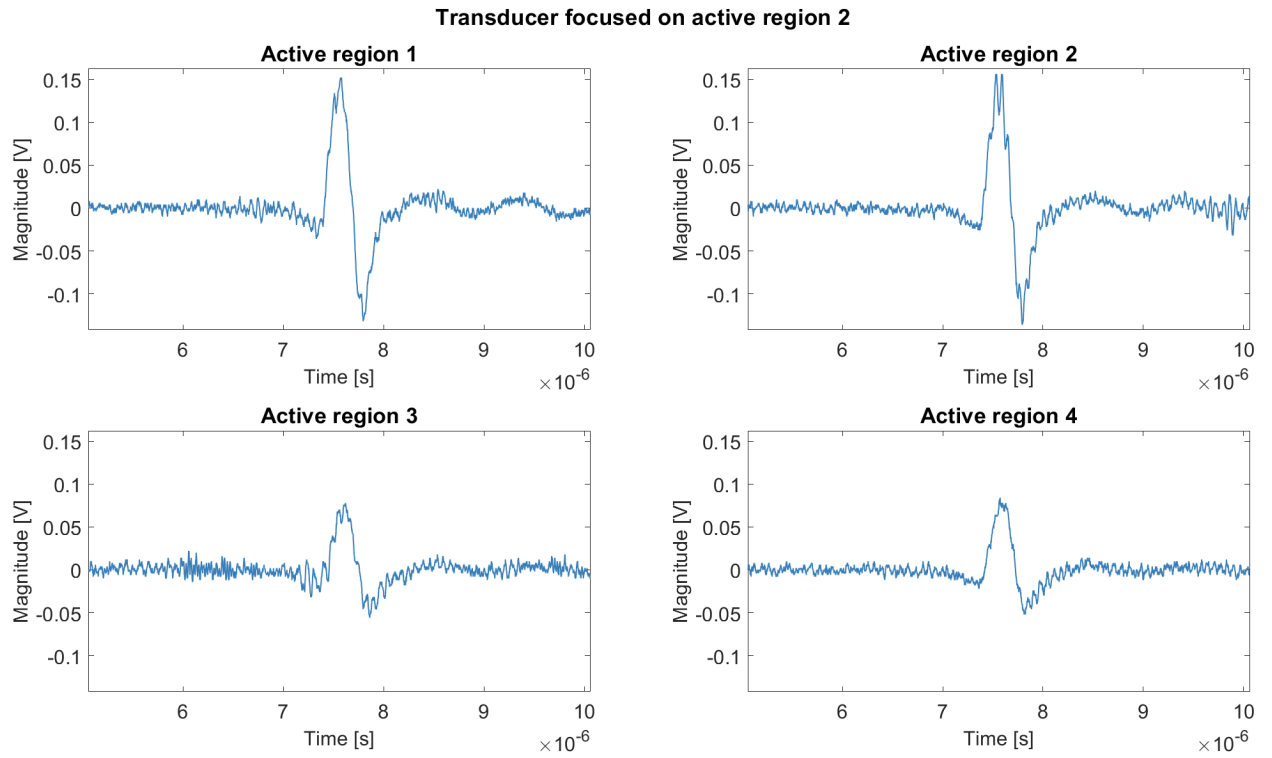


Figure 5.23: Transducer focused on active region 2, columns connected to ground and rows connected to signal. Unused wires are connected to earth.

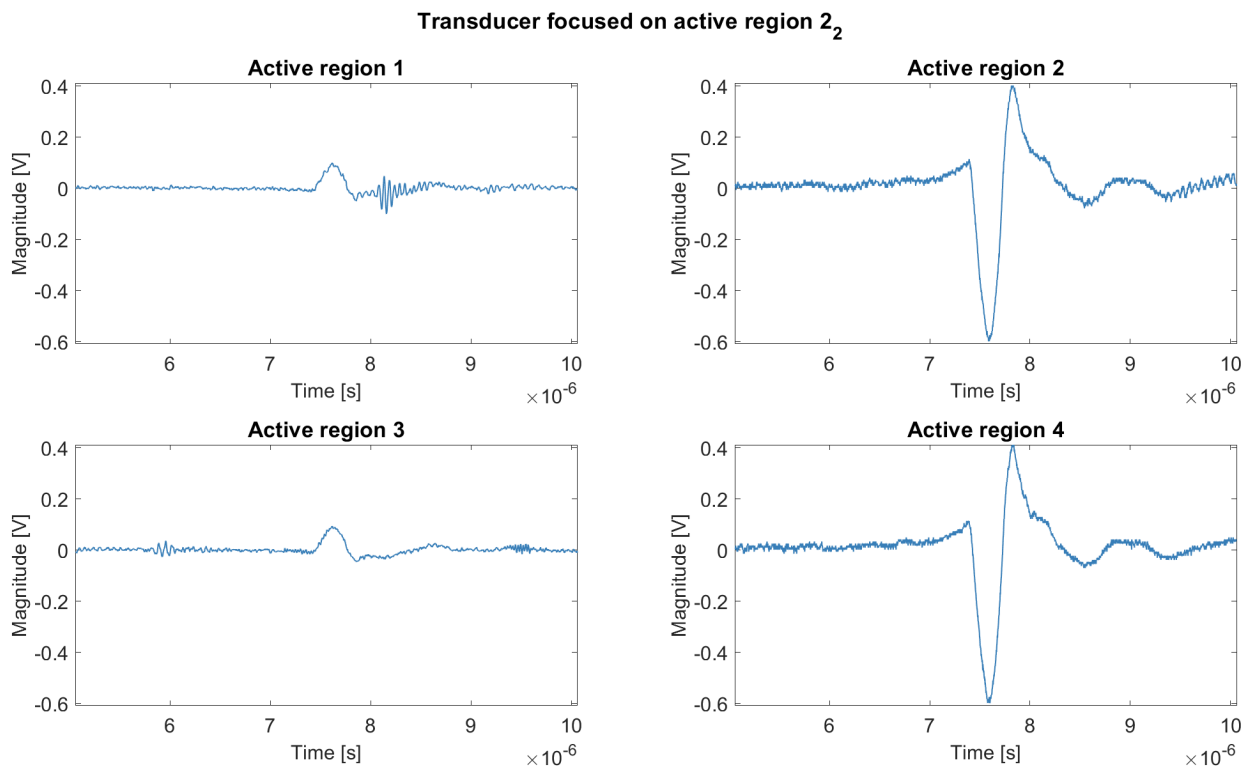


Figure 5.24: Transducer focused on active region 2, columns connected to signal and rows connected to ground. Unused wires are connected to earth.

5.2.8 Connecting 1 wire to earth

Then an experiment was performed to find out if all wires should be clamped to the table or if only one is also sufficient. In Figure 5.25 all combinations that were measured are shown. These measurements for region 1 are done for all the regions. The results of these measurements can be found in B.

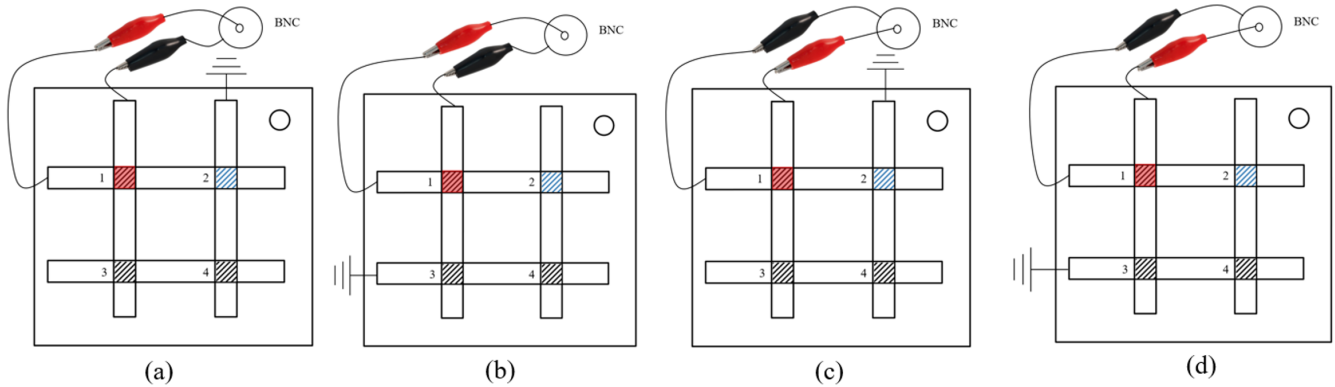


Figure 5.25: Transducer focused on active region 2, region 1 is measured.

This means that connecting the unmeasured Rows to earth has no effect on the measurements. But when the unmeasured columns are connected to earth there is a change in signal. When the rows are connected to the signal input of the BNC, the difference in rows could be determined.

5.2.9 Subtraction of the signals

Because the rows and columns could be distinguished, the region where the transducer is focused on could be determined. There are two ways this can be done; when the data is derived from the oscilloscope or when doing the data processing.

When subtracting the data on the oscilloscope two channels are needed. The setup for this measurement is shown in Figure 5.26. The row of interest is connected to the signal of the BNC with an alligator clip, the ground part is connected to the earth. This is also done for the columns. One of the signals is amplified by the 40 dB amplifier and one at 40 dB at the pulse receiver, the outputs are connected to channel 1 (CH1) and channel 2 (CH2) of the oscilloscope.

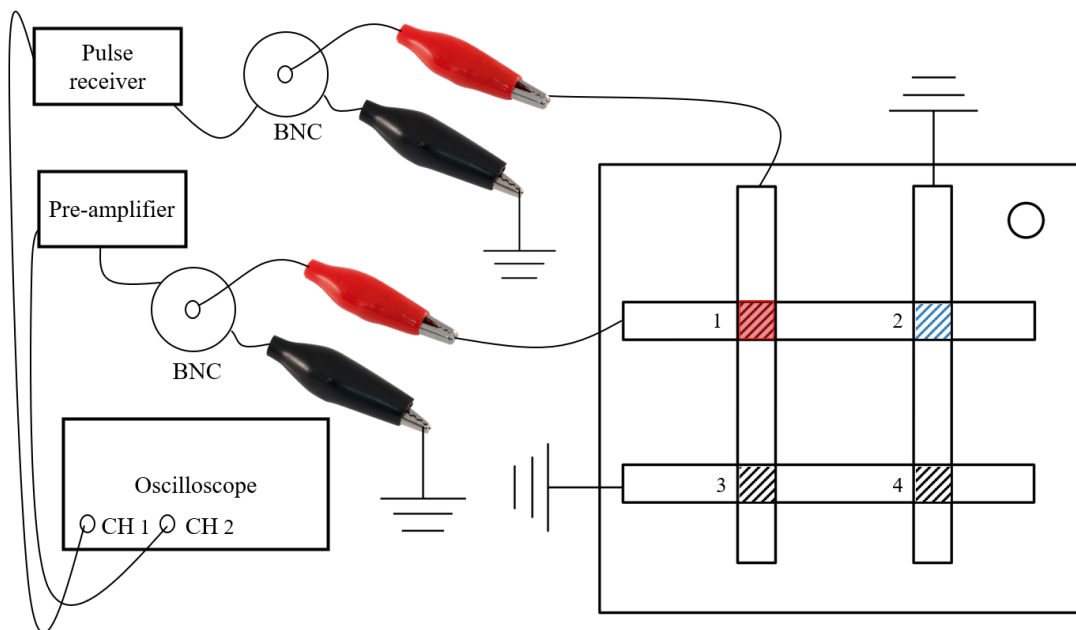


Figure 5.26: The setup for measuring two BNC signals from region 1 in the same time.

The results of these measurements can be found in Appendix C. When focusing on region 2 the bar graph for subtracting CH1- CH2 is highest for 2. That is what is expected when focusing on region 2 and expected. But when subtracting CH1-CH2 for region 4, region 2 is higher than region 4. Further on, it is remarkable that the amplitude for CH1 is higher than for CH2. In order to get a better result, the values should be normalized by dividing everything by the highest peak.

When referring to CH1 this means that the columns are connected to the signal, in CH2 the rows are connected to the signal, the same way as shown in Figure 5.26. Matlab is used to normalize the plots by dividing everything by the highest peak, meaning that when the transducer is focused on region 2 alle plots will be divided by the highest value of the peak from region 2. Then the values are subtracted, CH1 - CH2. After subtracting the peak to peak values of these plots are collected and plotted in a bar graph, Figure 5.27. The signals for focusing on region 1 were too noisy to obtain reliable values, that is the reason it differs from the graphs where the transducer focused on other regions. But when looking at 2, 3 and 4, the region where the transducer was focused on gives the highest peak which indicates that the transducer is focused on this region.

So it is possible to distinguish the region where the transducer is focused on when measuring two channels. When doing this real-time on the oscilloscope there are some drawbacks. First the amplitude for CH1 is much higher than for CH2 so subtracting it gives such a small difference that it isn't noticeable on the oscilloscope screen. Further on, the transducer is moved manually. So positioning the focus could differ on the regions, this could have an effect on the amplitude height of the signals. The distance between the transducer and the transparent transducer was always 20 mm, but it could be the case that this differs slightly, because the transducer was placed manually in the setup. This can cause a time delay, if the 2 signals of the active region are measured separately the subtraction would give not the right outcome.

There was a source which caused noise at random places in the signals. When this noise was in the recorded in the signal, the Matlab script which choose the highest value for normalization would take the value of this noise. To overcome this, the highest value of the peak was determined manually based on the plots. This is less accurate and is not doable when developing a larger transducer. The peak selection for the peak-to-peak values of the bar graphs was done with a Matlab script where the peaks had to be clicked with the mouse. This was necessary because of the noise, but can cause a deviation.

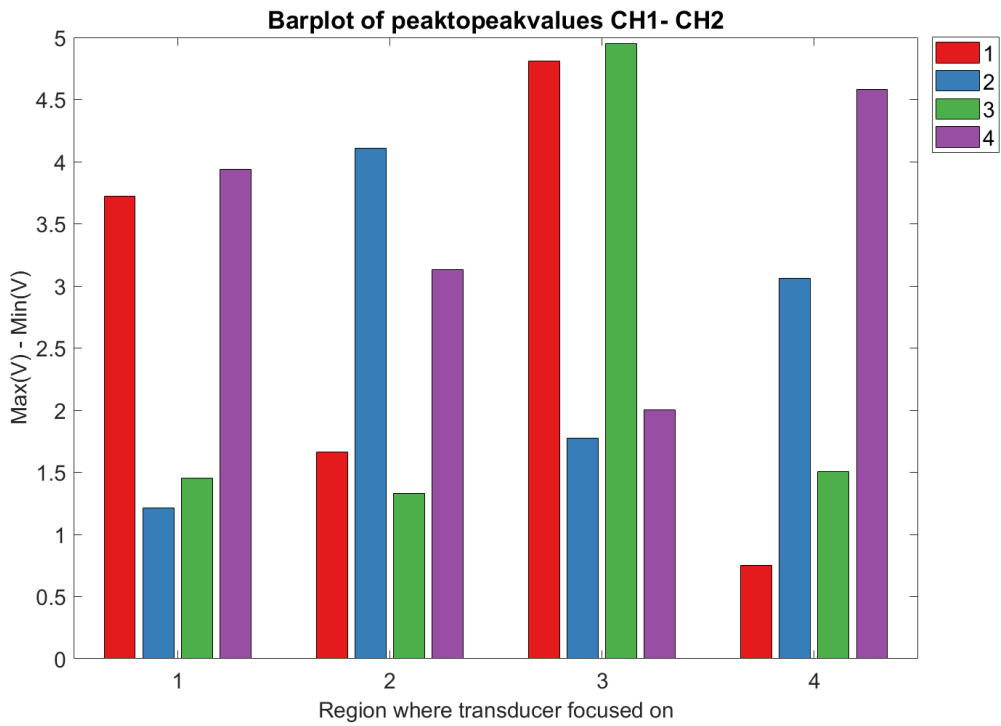


Figure 5.27: The bar graph when subtracting the signals after dividing CH1 and CH2 by their highest peak value.

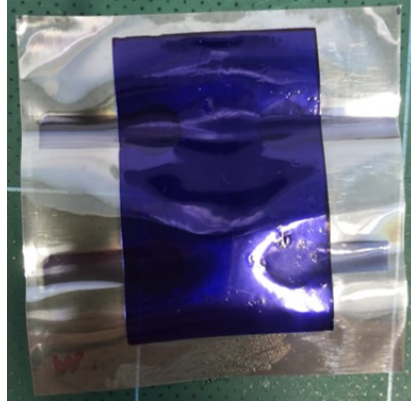
5.3 Prototype 3

There was a prototype developed which will not be effected by the earth problems. The positive side of the film has 4 dots with a diameter of 7 mm and an extension, Figure 5.28a. This extension is used to connect the copper wires. The negative side of the film has a rectangular shape ITO that covers all 4 dots, Figure 5.28b. In this way the back functions as a ground.

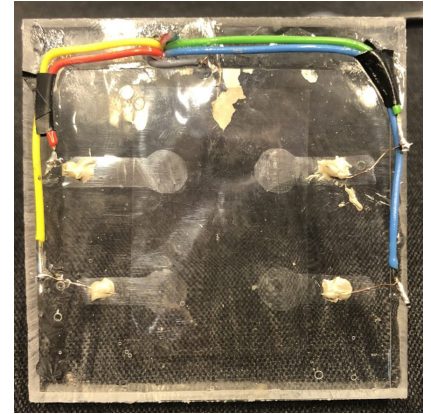
The prototype is shown in Figure 5.28c. Where the active regions are: Red; active side 1, Green; active side 2, Yellow; active side 3 and Blue; active side 4. A gray wire was attached to the negative side/ the back of the film.



(a) The PVDF film with PDF attached, positive side/ front.



(b) The PVDF film with PDF attached, negative side/ back.



(c) Prototype 3.

Figure 5.28: PVDF film with PDF for Prototype 3. The active regions are: Red; active side 1, Green; active side 2, Yellow; active side 3 and Blue; active side 4. A gray wire was attached to the negative side/ the back of the film.

The 2.25 MHz focused transducer focused on all regions, a bar graph was made to compare the sensitivity for all regions, see Figure 5.29. The signal of the region where the transducer was focused on gave the highest signal compared to the others. However, there is variation in sensitivity for the four regions. Region 4 has the highest sensitivity and then 2, 3, 1.

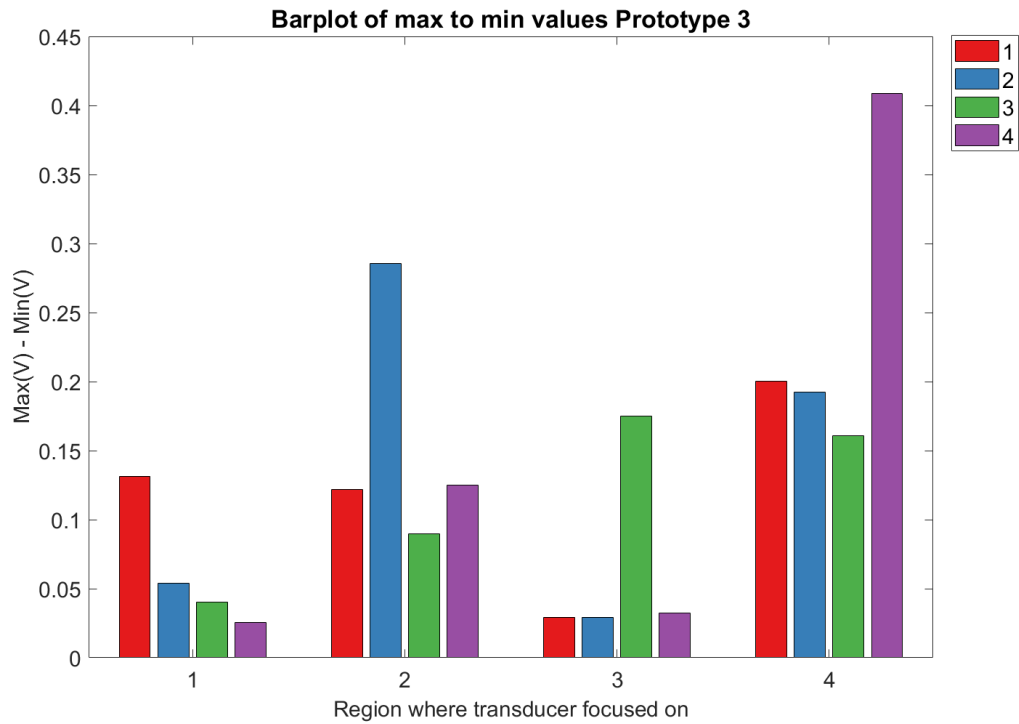


Figure 5.29: Bar graph of Prototype 3

The gray wire is attached to the back of the film. This is used as the ground of the BNC. Three things were tested:

1. Connecting the ground of the BNC to the table, the signal to one of the active regions.
2. Connecting the ground of the BNC to the gray wire, the signal to one of the active regions.
3. Connecting the ground of the BNC to the earth and the gray wire, the signal to one of the active regions.

The transducer was focused at region 3, this gave the highest signal compared to the other regions in every case. Further on, the signals had the same shape and amplitude for all 3 measurements. However, when only connecting the gray wire to the ground (case 2), the signal was very noisy.

Chapter 6 Conclusions and outlook

In this chapter the conclusions of this thesis are mentioned, next to an outlook with recommendations for further research.

The research question was; "How to make a two by two array transparent ultrasound transducer using PVDF coated with ITO?"

6.1 Conclusions

6.1.1 Transducer development

The protocol for making the transducer is described in Section 3.5. In order to make this protocol some things were concluded. First the substrate was determined, PMMA was chosen because it was used before in other transparent transducers, and it has good impedance matching with PVDF. Then an adhesive was chosen, this became NOA85V. NOA85V has a large range in optical transmission, and it was easy to work with since it was based on one component and had a low viscosity. However the viscosity was so low that when applying the film on the substrate, the epoxy would be pushed away from under the film. This problem was solved by clearing the epoxy in 2 steps.

The dimensions for the PVDF film was 55x55 mm, with 5 mm width ITO ribbons as electrodes. By choosing this electrode width, the PDF was easy to cut in shape. Further on, the PVDF size was sufficient to examine the crosstalk and to prove the transparent transducer of these materials work. The dimensions of the PMMA became 65x65x8 mm. There was 10 mm left at the top and the right side to let the wires run over. 8 mm thickness was chosen to delay the internal reflections in a great extent.

The ITO could be removed when washed in 1% HCl for 2 minutes. To remove ITO selectively, PDF should be attached to the film, heating the film was necessary for good adhesion between the PDF and PVDF film. The PDF was removed when exposing to 1% NaOH for approximately 20 minutes.

The procedure of selectively removing ITO damaged the film and decreased the amplitude of the signal around 3 times. However, there was still a significant signal left.

6.1.2 Testing transparent transducer

The movable transducer was focused onto multiple regions. When focusing on a region without ITO the signal was more than 10 times lower than when it was focused on an active region. So the transmittance in the PVDF film is very limited. When the transducer was focused on regions with 1 side of ITO it could give significant signal because the electrodes work as capacitors in a line integral. However it is lower than when is focussed on the active regions. In further research, this behavior should be examined more, with the goal to compensate for this.

When testing the transparent transducer, the columns differ in every case and the rows do not. Except when the row was connected to the transducer and the unmeasured column was connected to the earth.

In order to determine on which active region the transducer is focused on. The column and the row of interest should go to the signal of separate BNC's, the column that isn't used should be connected to earth. In the first case the columns differ and in the second case the rows differ. But in both cases the region

of interest has the highest amplitude. A Matlab script was made to normalize the amplitudes in both scenario's. Then the signals were subtracted and the active region where the transducer was focused on is found. The ITO coating from the columns was on the back (/negative side) of the PVDF film and the ITO coating from the rows was on the front (/positive side) of the PVDF film.

6.2 Outlook

The shape of the PMMA could also be made like a prism, as suggested in Section 2.2.2. This is done before and useful to get rid of internal reflections. This was not done in this thesis, because sawing the PMMA in that shape would give lots of light scattering at the surface. However when light is shined on a large surface at once this may not be sufficient. The difference in thickness causes delays and the CTC is more difficult to track.

When making ITO electrodes with a much smaller width, cutting the PDF in the desired shape will be much more difficult. This can be overcome by using a metal mask. This mask will have a pattern of the ITO electrodes. The PDF can be attached to the PVDF fully, when placing the PVDF in the UV source the mask is applied. After UV exposure is done, the PDF that was protected by the mask should be washed away (with sodium carbonate for example [44]). The PDF that was exposed to UV light will remain. This has to be done twice, for both sides. This mask can be made using a laser cutter machine and the ITO shape will be very precise.

In order to reduce the damage to the performance of the PVDF film by the procedure, low concentrated KOH might be considered. It could take a long time for the PDF to come off, but if it gives less damage it could be worthwhile.

The active region is measured with the signal of the row and column of that region. These amplitudes differ in a great extent, so when subtracting the signals the difference between the rows is almost unnoticeable. An opamp could be used to overcome this problem, both signals could be connected to the opamp with different resistors in between to compensate for the amplitude difference. The opamp could then subtract the signals before the oscilloscope, so only one channel is needed to measure the region.

The sensitivity of the regions differs a bit, it should be investigated how much the sensitivity of every active region is, then this could be compensated.

In the future, it is desired to measure all regions at once and expand the transducer with more active regions. Measuring all those regions will not be possible with an oscilloscope with only 2 channels. So a new setup should be made to measure and then compares all regions.

The column/ ribbon at the negative side of the PVDF film that is not measured should be connected to the earth to get a signal from the rows/ ribbon at the positive side of the PVDF film. When making a larger transducer, for example a 3x3 array transducer, an experiment could be performed to find out if all columns that aren't measured should be connected to earth or if only one column is enough [51].

The hypothesis was that based on the time shift of the signals from the active regions, the CTC's could be located. However the electrode ribbons work like a capacitor and therefore the whole line is integrated at the same time. Therefore it is not possible to look at time shift, but the amplitude of the subtracted signal should make it possible to locate the CTC.

In this research, the focussed transducer was placed at 20 mm from the active region. And it is known where the signal is coming from. In the future, the width of the acoustic wave and the amplitude of the signal should be used to determine the depth and the location of the CTC.

Bibliography

- [1] Yun He et al. “In vivo label-free photoacoustic flow cytography and on-the-spot laser killing of single circulating melanoma cells”. In: *Nature* 6 (2016), p. 39616. DOI: 10.1038/srep39616. URL: <https://doi.org/10.1038/srep39616>.
- [2] Danyang Ren et al. “A Review of Transparent Sensors for Photoacoustic Imaging Applications”. In: *Photonics* 8.8 (2021). ISSN: 2304-6732. DOI: 10.3390/photonics8080324. URL: <https://www.mdpi.com/2304-6732/8/8/324>.
- [3] Rabindra. Yadav. “Definitions in laser technology”. In: *Journal of Cutaneous and Aesthetic Surgery* 2.1 (2009), pp. 45–46. DOI: 10.4103/0974-2077.53103. eprint: <https://www.jcasonline.com/article.asp?issn=0974-2077;year=2009;volume=2;issue=1;spage=45;epage=46;aulast=Yadav;t=6>. URL: <https://www.jcasonline.com/article.asp?issn=0974-2077;year=2009;volume=2;issue=1;spage=45;epage=46;aulast=Yadav;t=6>.
- [4] F. Xu et al. “Mathematical Modeling of Skin Bioheat Transfer”. In: *Applied Mechanics Reviews* 62.5 (July 2009). 050801. ISSN: 0003-6900. DOI: 10.1115/1.3124646. eprint: <https://asmedigitalcollection.asme.org/appliedmechanicsreviews/article-pdf/62/5/050801/5442612/050801.pdf>. URL: <https://doi.org/10.1115/1.3124646>.
- [5] T. Buma, M. Spisar, and M. O’Donnell. “High-frequency ultrasound array element using thermoelastic expansion in an elastomeric film”. In: *Applied Physics Letters* 79.4 (2001), pp. 548–550. DOI: 10.1063/1.1388027. eprint: <https://doi.org/10.1063/1.1388027>. URL: <https://doi.org/10.1063/1.1388027>.
- [6] Hailey Olds et al. *Is photoacoustic imaging clinically safe: Evaluation of possible thermal damage due to laser-tissue interaction*. URL: https://digitalcommons.wayne.edu/som_srs/56/.
- [7] Terence T. W. Wong et al. “Label-free automated three-dimensional imaging of whole organs by microtomy-assisted photoacoustic microscopy”. In: *Nature Communications* 1386.8 (2017). DOI: 10.1038/s41467-017-01649-3. URL: <https://www.sciencedirect.com/science/article/pii/S0009250910007323>.
- [8] Mohammad Mehrmohammadi et al. “Photoacoustic Imaging for Cancer Detection and Staging”. In: *Current Molecular Imaging (Discontinued)* 2.1 (2013), pp. 89–105. ISSN: 2211-5552/2211-5544. DOI: 10.2174/2211555211302010010. URL: <http://www.eurekaselect.com/article/49703>.
- [9] Galanzha EI et al. “In vivo magnetic enrichment and multiplex photoacoustic detection of circulating tumour cells”. In: *Nat Nanotechnol.* 4.12 (2009), pp. 855–860. DOI: 10.1038/nnano.2009.333.
- [10] John A Viator et al. “Gold nanoparticle mediated detection of prostate cancer cells using photoacoustic flowmetry with optical reflectance”. In: *J Biomed Nanotechnol.* 6.2 (2010), pp. 187–191. DOI: 10.1166/jbn.2010.1105.
- [11] Tomasz Borowski. “Photoacoustic in remote sensing”. In: *Radioelectronic Systems Conference 2019*. Ed. by Piotr Kaniewski and Jan Matuszewski. Vol. 11442. International Society for Optics and Photonics. SPIE, 2020, pp. 342–352. DOI: 10.1117/12.2565308. URL: <https://doi.org/10.1117/12.2565308>.
- [12] Khoa Pham et al. “Broadband All-Optical Plane-Wave Ultrasound Imaging System Based on a Fabry–Perot Scanner”. In: *IEEE Transactions on Ultrasonics, Ferroelectrics, and Frequency Control* 68.4 (2021), pp. 1007–1016. DOI: 10.1109/TUFFC.2020.3028749.

- [13] R. Ansari et al. “All-optical endoscopic probe for high resolution 3D photoacoustic tomography”. In: *Photons Plus Ultrasound: Imaging and Sensing 2017*. Ed. by Alexander A. Oraevsky and Lihong V. Wang. Vol. 10064. International Society for Optics and Photonics. SPIE, 2017, pp. 276–281. DOI: 10.1117/12.2250617. URL: <https://doi.org/10.1117/12.2250617>.
- [14] Josue E. Muñoz-Pérez et al. “Fabry-Perot interferometric sensor to measuring vibrations in mechanical structures based on the Doppler effect”. In: *Applied Optical Metrology IV*. Ed. by Erik Novak, James D. Trolinger, and Christopher C. Wilcox. Vol. 11817. International Society for Optics and Photonics. SPIE, 2021, pp. 64–69. DOI: 10.1117/12.2594979. URL: <https://doi.org/10.1117/12.2594979>.
- [15] Hao Li et al. “A transparent broadband ultrasonic detector based on an optical micro-ring resonator for photoacoustic microscopy”. In: *Scientific Reports* 4.1 (2014). DOI: 10.1038/srep04496.
- [16] Zhenhao Li, Afshin Kashani Ilkhechi, and Roger Zemp. “Transparent capacitive micromachined ultrasonic transducers (CMUTs) for photoacoustic applications”. In: *Opt. Express* 27.9 (2019), pp. 13204–13218. DOI: 10.1364/OE.27.013204. URL: <http://opg.optica.org/oe/abstract.cfm?URI=oe-27-9-13204>.
- [17] J.J. Niederhauser et al. “Transparent ITO coated PVDF transducer for optoacoustic depth profiling”. In: *Optics Communications* 253.4 (2005), pp. 401–406. ISSN: 0030-4018. DOI: <https://doi.org/10.1016/j.optcom.2005.05.005>. URL: <https://www.sciencedirect.com/science/article/pii/S0030401805004542>.
- [18] Cheng Fang, He Hu, and Jun Zou. “A Focused Optically Transparent PVDF Transducer for Photoacoustic Microscopy”. In: *IEEE Sensors Journal* 20.5 (2020), pp. 2313–2319. DOI: 10.1109/JSEN.2019.2952971.
- [19] Elias Blumenröther et al. “Single Transparent Piezoelectric Detector for Optoacoustic Sensing—Design and Signal Processing”. In: *Sensors* 19.9 (2019). ISSN: 1424-8220. DOI: 10.3390/s19092195. URL: <https://www.mdpi.com/1424-8220/19/9/2195>.
- [20] K.A. Snook et al. “Design, fabrication, and evaluation of high frequency, single-element transducers incorporating different materials”. In: *IEEE Transactions on Ultrasonics, Ferroelectrics, and Frequency Control* 49.2 (2002), pp. 169–176. DOI: 10.1109/58.985701.
- [21] Ya-Han Liu et al. “Transparent Flexible Piezoelectric Ultrasound Transducer for Photoacoustic Imaging System”. In: *IEEE Sensors Journal* 22.3 (2022), pp. 2070–2077. DOI: 10.1109/JSEN.2021.3135872.
- [22] Kanae Mukai PhD et al. “Safety of Venipuncture Sites at the Cubital Fossa as Assessed by Ultrasonography”. In: *Journal of Patient Safety* 16.1 (2020), pp. 98–105. DOI: 10.1097/PTS.0000000000000441.
- [23] Elaine N. Marieb and Katja Hoehn. *Human anatomy & physiology*. 11th ed. Pearson Education Limited, 2019. ISBN: 9781292260853.
- [24] Wanjia Gao et al. “Study of Ultrasonic Near-Field Region in Ultrasonic Liquid-Level Monitoring System”. In: *Micromachines* 11 (Aug. 2020), p. 763. DOI: 10.3390/mi11080763.
- [25] Wenfeng Xia et al. “A new acoustic lens material for large area detectors in photoacoustic breast tomography”. In: *Photoacoustics* 1 (May 2013). DOI: 10.1016/j.pacs.2013.05.001.
- [26] Matthew Kyrish et al. “Ultra-slim plastic endomicroscope objective for non-linear microscopy”. In: *Opt. Express* 19.8 (2011), pp. 7603–7615. DOI: 10.1364/OE.19.007603. URL: <http://opg.optica.org/oe/abstract.cfm?URI=oe-19-8-7603>.
- [27] J. Lubbers and R. Graaff. “A simple and accurate formula for the sound velocity in water”. In: *Ultrasound in Medicine Biology* 24.7 (1998), pp. 1065–1068. ISSN: 0301-5629. DOI: 10.1016/S0301-5629(98)00091-X. URL: <https://www.sciencedirect.com/science/article/pii/S030156299800091X>.
- [28] Thomas J. Allen, Edward Zhang, and Paul C. Beard. “Fully parallelised read-out of a Fabry-Perot ultrasound sensor using an InGaAs camera for fast photoacoustic imaging (Conference Presentation)”. In: *Photons Plus Ultrasound: Imaging and Sensing 2020*. Ed. by Alexander A. Oraevsky and Lihong V. Wang. Vol. 11240. International Society for Optics and Photonics. SPIE, 2020. DOI: 10.1117/12.2550127. URL: <https://doi.org/10.1117/12.2550127>.

- [29] Long-Hua Lee and Wen-Chang Chen. “High-Refractive-Index Thin Films Prepared from Trialkoxysilane-Capped Poly(methyl methacrylate)Titania Materials”. In: *Chemistry of Materials* 13.3 (2001), pp. 1137–1142. DOI: 10.1021/cm000937z. URL: <https://doi.org/10.1021/cm000937z>.
- [30] Caroline Boudoux. “Fundamentals of Biomedical Optics”. In: *Fundamentals of Biomedical Optics*. École Polytechnique Montréal. Pollux, 2016. ISBN: 978-1366446190.
- [31] Polymer database. Accessed: 2022-07-09. URL: <https://polymerdatabase.com/polymer%20physics/Ref%20Index%20Table2%20.html>.
- [32] *Norland Optical Adhesive 85*. Technical data sheet, 2022. Norland Products Incorporated.
- [33] Norland Products. *Norland Optical Adhesive 85V*. 2022. URL: <https://www.norlandprod.com/adhesives/NOA85V.html> (visited on 05/06/2022).
- [34] INC. EPOXY TECHNOLOGY. *EPO-TEK 301 Technical data sheet*. Accessed: 2022-06-03. 2012. URL: <https://i-fiberoptics.com/pdf/epo-tek.pdf>.
- [35] Thomas L. Szabo. “Chapter 5 - Transducers”. In: *Diagnostic Ultrasound Imaging: Inside Out (Second Edition)*. Ed. by Thomas L. Szabo. Second Edition. Boston: Academic Press, 2014, pp. 121–165. ISBN: 978-0-12-396487-8. DOI: 10.1016/B978-0-12-396487-8.00005-7. URL: <https://www.sciencedirect.com/science/article/pii/B9780123964878000057>.
- [36] *PVDF Piezoelectric Film Optically Transparent, Technical data sheet. 48 μ m thick PVDF with ITO coating*, 2022. PolyK Technologies.
- [37] Marcos S. Martins et al. “Wideband and Wide Beam Polyvinylidene Difluoride (PVDF) Acoustic Transducer for Broadband Underwater Communications”. In: *Sensors* 19.18 (2019). ISSN: 1424-8220. DOI: 10.3390/s19183991. URL: <https://www.mdpi.com/1424-8220/19/18/3991>.
- [38] J. Inderherbergh. “Polyvinylidene Fluoride (PVDF) Appearance, General Properties and Processing”. In: *Ferroelectrics* 115.4 (1991), pp. 295–302. DOI: 10.1080/00150193.1991.11876614. eprint: <https://doi.org/10.1080/00150193.1991.11876614>. URL: <https://doi.org/10.1080/00150193.1991.11876614>.
- [39] Acoplastic. *PVDF is UV-resistant and can withstand chemical and mechanical loads*. Accessed 2022-07-10. 2021. URL: <https://acoplastic.com/high-tech-and-construction-plastic/pvdf-en/>.
- [40] Robert L. Crane, John Hart-Smith, and John Newman. “8 - Nondestructive inspection of adhesive bonded joints”. In: *Adhesive Bonding (Second Edition)*. Ed. by Robert D. Adams. Second Edition. Woodhead Publishing Series in Welding and Other Joining Technologies. Woodhead Publishing, 2021, pp. 215–256. ISBN: 978-0-12-819954-1. DOI: 10.1016/B978-0-12-819954-1.00008-3. URL: <https://www.sciencedirect.com/science/article/pii/B9780128199541000083>.
- [41] C.J Huang, Y.K Su, and S.L Wu. “The effect of solvent on the etching of ITO electrode”. In: *Materials Chemistry and Physics* 84.1 (2004), pp. 146–150. DOI: 10.1016/j.matchemphys.2003.11.021. URL: <https://doi.org/10.1016/j.matchemphys.2003.11.021>.
- [42] Jae-Hyeok Choi et al. “Acid-catalyzed kinetics of indium tin oxide etching”. In: *Thin Solid Films* 565 (2014), pp. 179–185. ISSN: 0040-6090. DOI: 10.1016/j.tsf.2014.06.053. URL: <https://www.sciencedirect.com/science/article/pii/S0040609014007172>.
- [43] Suelene S. Mammana et al. “Study of wet etching thin films of indium tin oxide in oxalic acid by monitoring the resistance”. In: *Thin Solid Films* 567 (2014), pp. 20–31. ISSN: 0040-6090. DOI: 10.1016/j.tsf.2014.07.027. URL: <https://www.sciencedirect.com/science/article/pii/S0040609014007482>.
- [44] National Chiao Tung University. Accessed: 2022-07-09. 2005. URL: <https://ir.nctu.edu.tw/bitstream/11536/74691/7/851507.pdf>.
- [45] Yuan-Chien Tsai et al. “Fabrication of microfluidic devices using dry film photoresist for microchip capillary electrophoresis”. In: *Journal of Chromatography A* 1111.2 (2006). 18th International Symposium on MicroScale Bioseparations, pp. 267–271. ISSN: 0021-9673. DOI: 10.1016/j.chroma.2005.12.003. URL: <https://www.sciencedirect.com/science/article/pii/S002196730502385X>.
- [46] Mei Jiun Lee et al. “Degradation of PVDF-based composite membrane and its impacts on membrane intrinsic and separation properties”. In: *Journal of Polymer Engineering* 36.3 (2016), pp. 261–268. DOI: doi:10.1515/polyeng-2015-0064. URL: <https://doi.org/10.1515/polyeng-2015-0064>.

- [47] Jean E. Marshall et al. “On the Solubility and Stability of Polyvinylidene Fluoride”. In: *Polymers* 13.9 (2021). ISSN: 2073-4360. DOI: 10.3390/polym13091354. URL: <https://www.mdpi.com/2073-4360/13/9/1354>.
- [48] N. Awanis Hashim, Yutie Liu, and K. Li. “Stability of PVDF hollow fibre membranes in sodium hydroxide aqueous solution”. In: *Chemical Engineering Science* 66.8 (2011), pp. 1565–1575. ISSN: 0009-2509. DOI: 10.1016/j.ces.2010.12.019. URL: <https://www.sciencedirect.com/science/article/pii/S0009250910007323>.
- [49] Formlabs. *Form wash and form cure: Automated post-processing*. Accessed: 2022-07-10. URL: <https://formlabs.com/eu/post-processing/wash-cure/>.
- [50] Tektronix. *How to use an oscilloscope: Complete Setup Guide: Tektronix*. Accessed: 2022-07-10. URL: <https://www.tek.com/en/documents/primer/setting-and-using-oscilloscope>.
- [51] Christian Rendl et al. “PyzoFlex: Printed Piezoelectric Pressure Sensing Foil”. In: Oct. 2012. DOI: 10.1145/2380116.2380180.

Appendix A Ground swapped

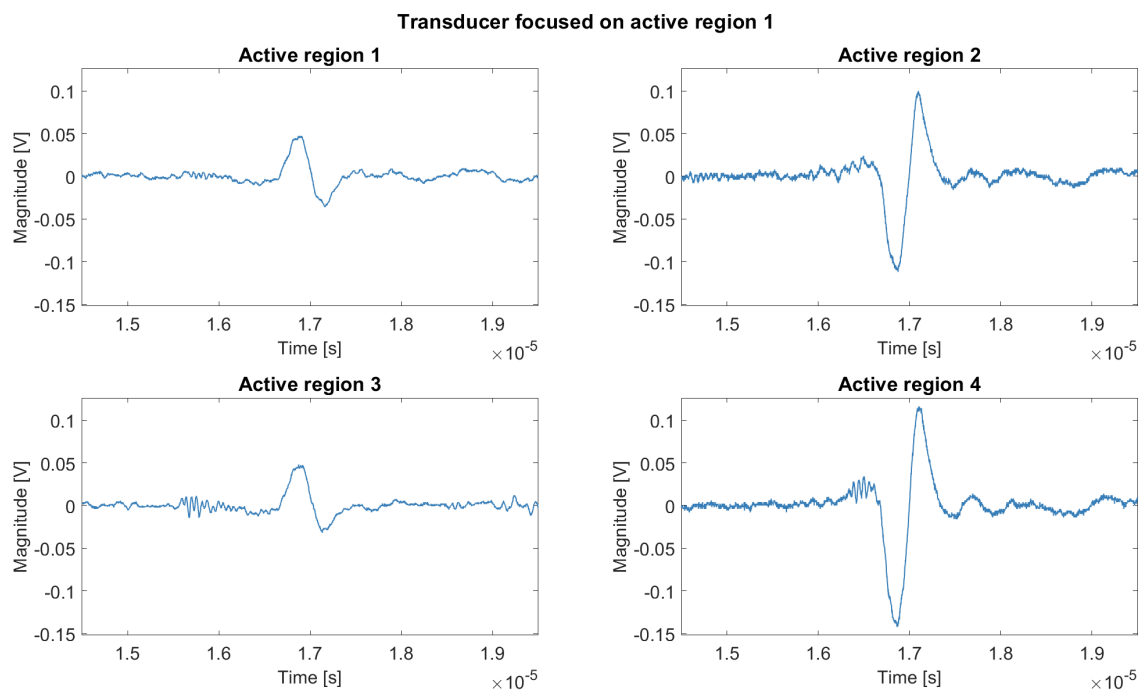


Figure A.1: The ground of transparent transducer is swapped, the transducer is focused on region 1.

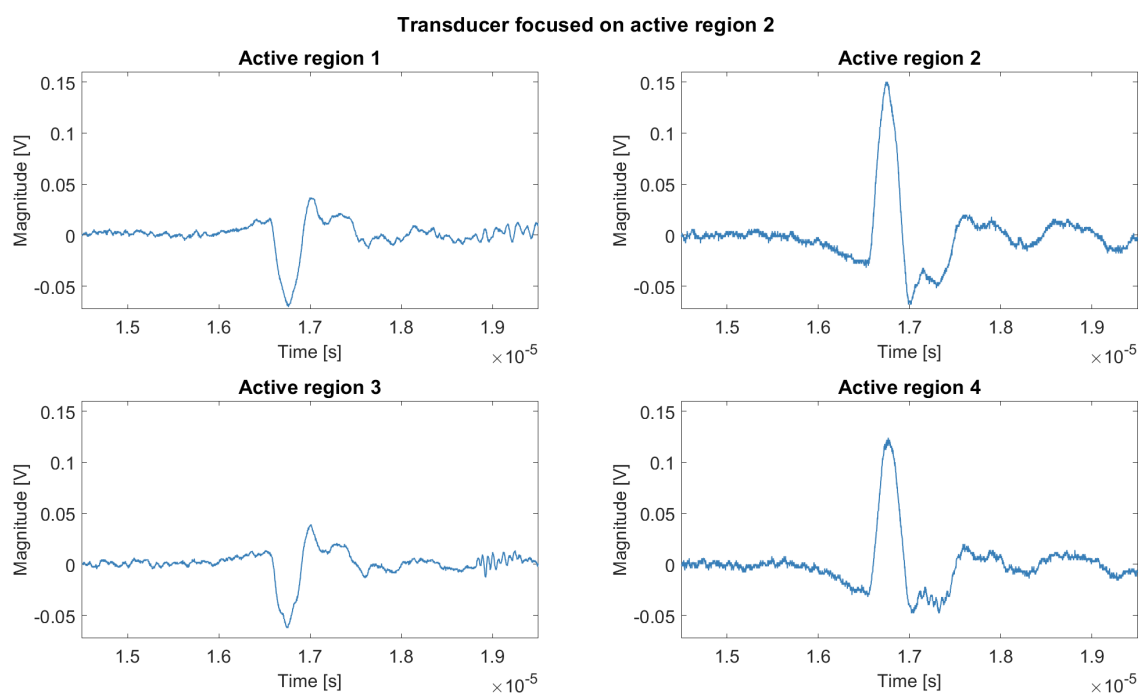


Figure A.2: The ground of transparent transducer is swapped, the transducer is focussed on region 2.

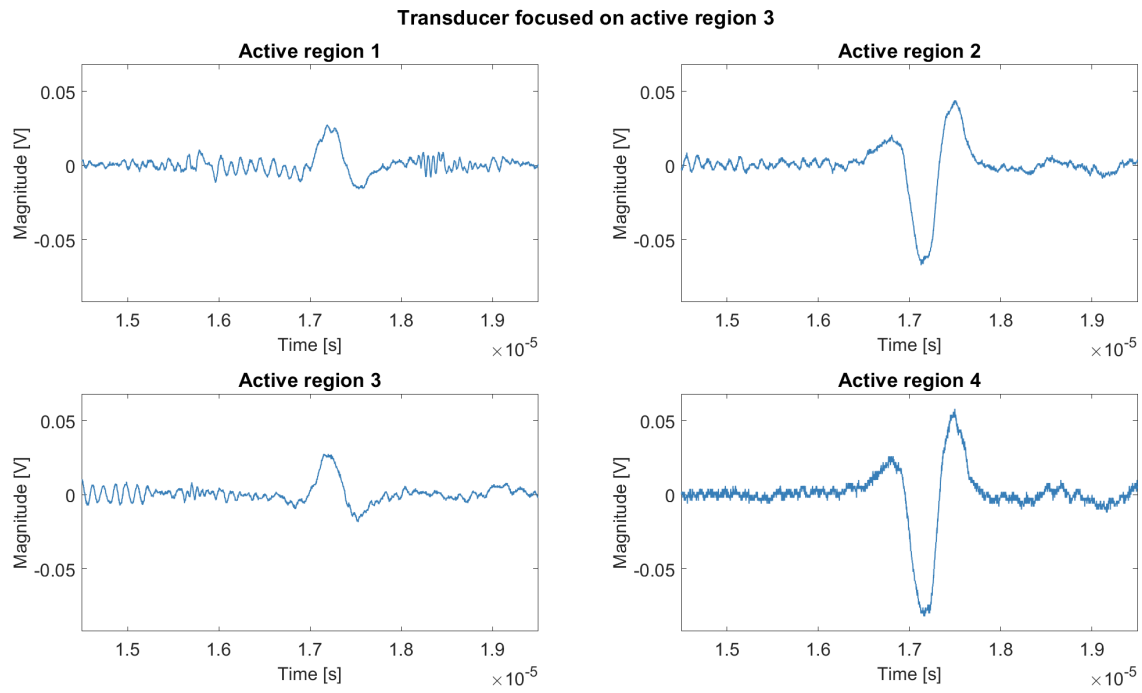


Figure A.3: The ground of transparent transducer is swapped, the transducer is focused on region 3.

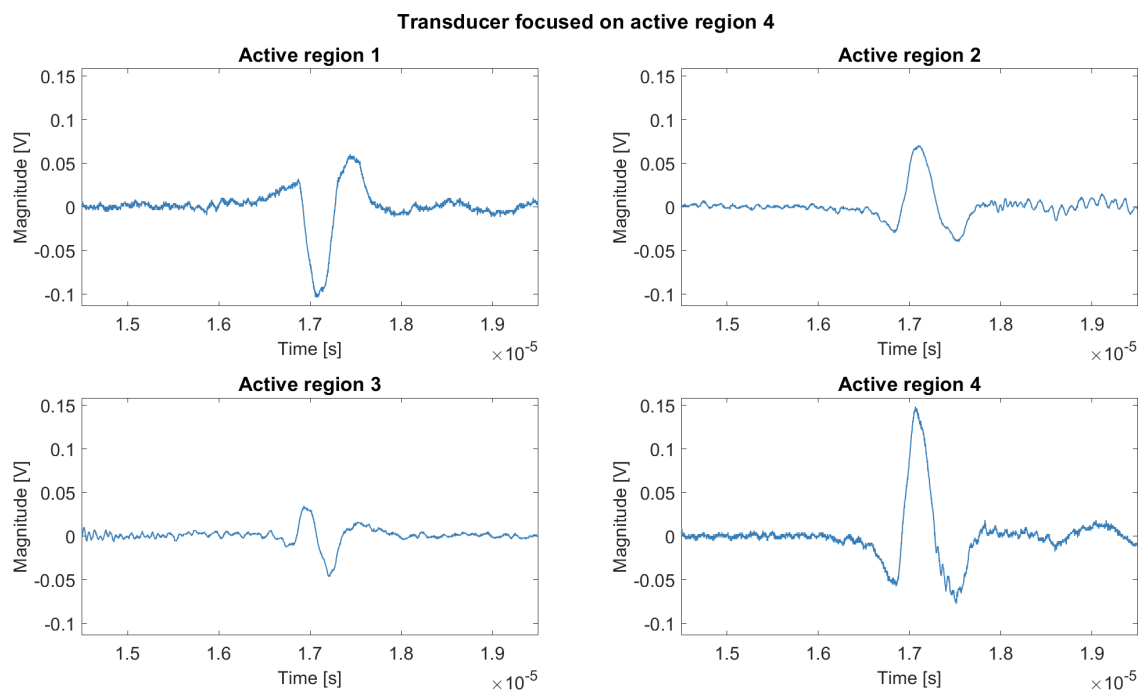


Figure A.4: The ground of transparent transducer is swapped, the transducer is focussed on region 4.

Appendix B Figures regarding grounding

Ground	Signal	Earth	Figure
Column	Row	columns and rows	Figure B.1
Rows	Columns	columns and rows	Figure B.2
Column	Row	non	Figure B.3
Row	Column	non	Figure B.4
Column	Row	Column	Figure B.5
Row	Column	Column	Figure B.7
Column	Row	Row	Figure B.6
Row	Column	Row	Figure B.8

Table B.1: Experiments regarding earth connections and Figure references.

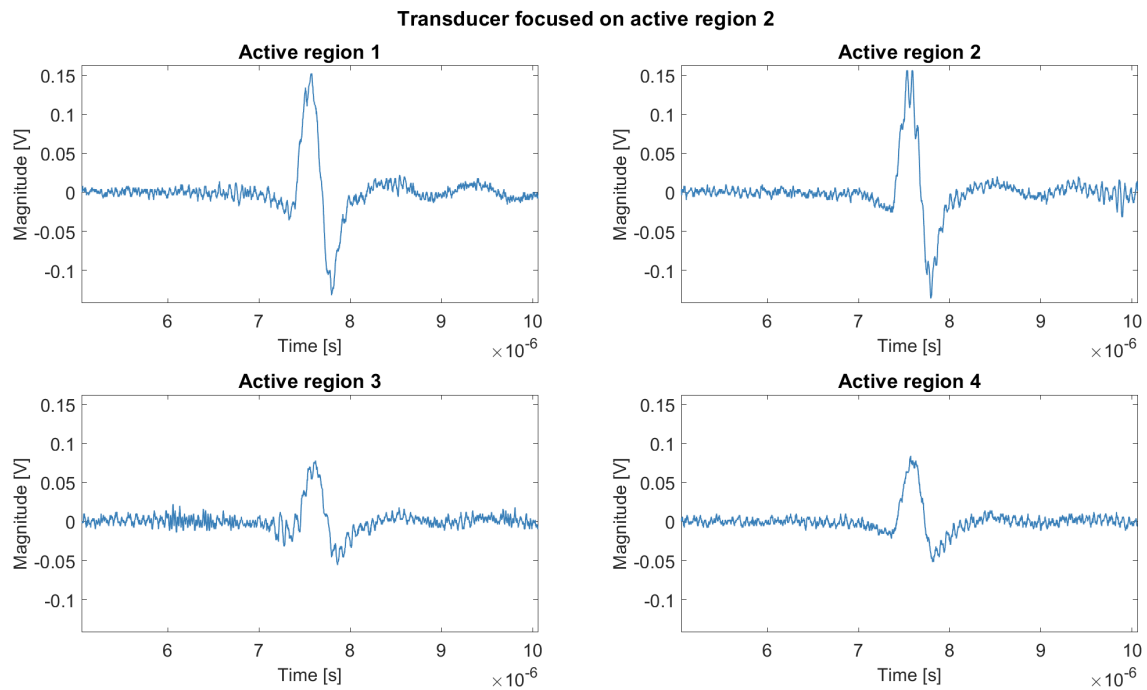


Figure B.1: Transducer focused on active region 2, rows to the signal of the BNC and columns to the ground of the BNC. The wires that aren't measured are connected to earth.

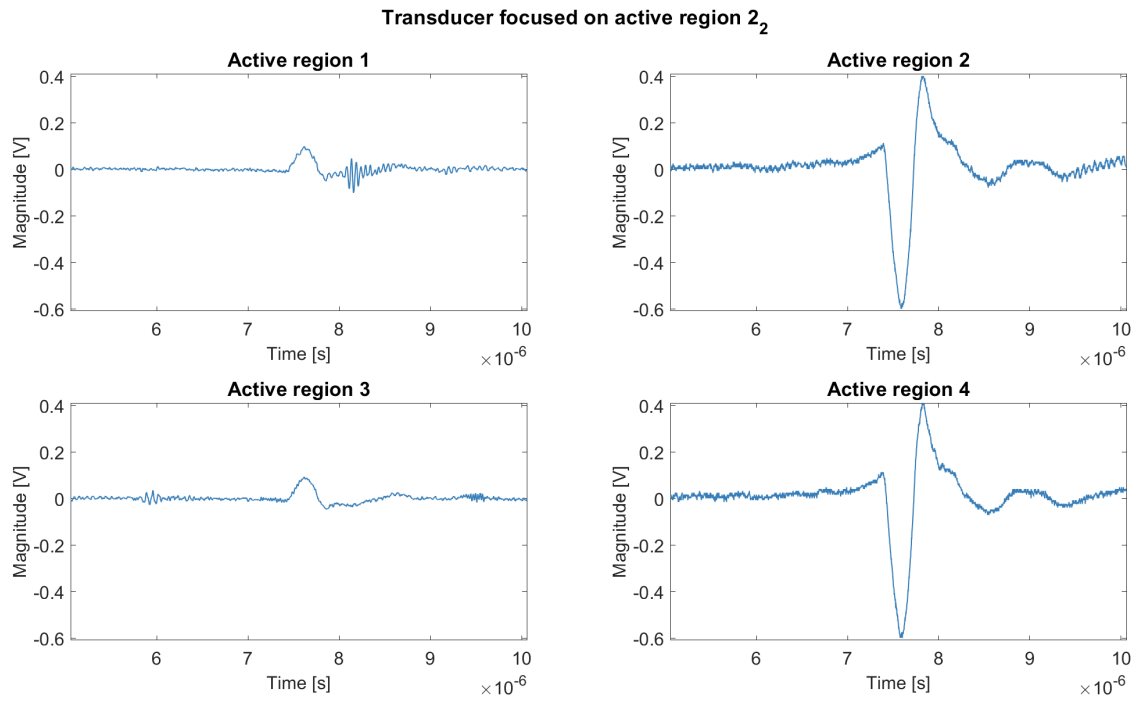


Figure B.2: Transducer focused on active region 2, columns to the signal of the BNC and rows to the ground of the BNC. The wires that aren't measured are connected to earth.

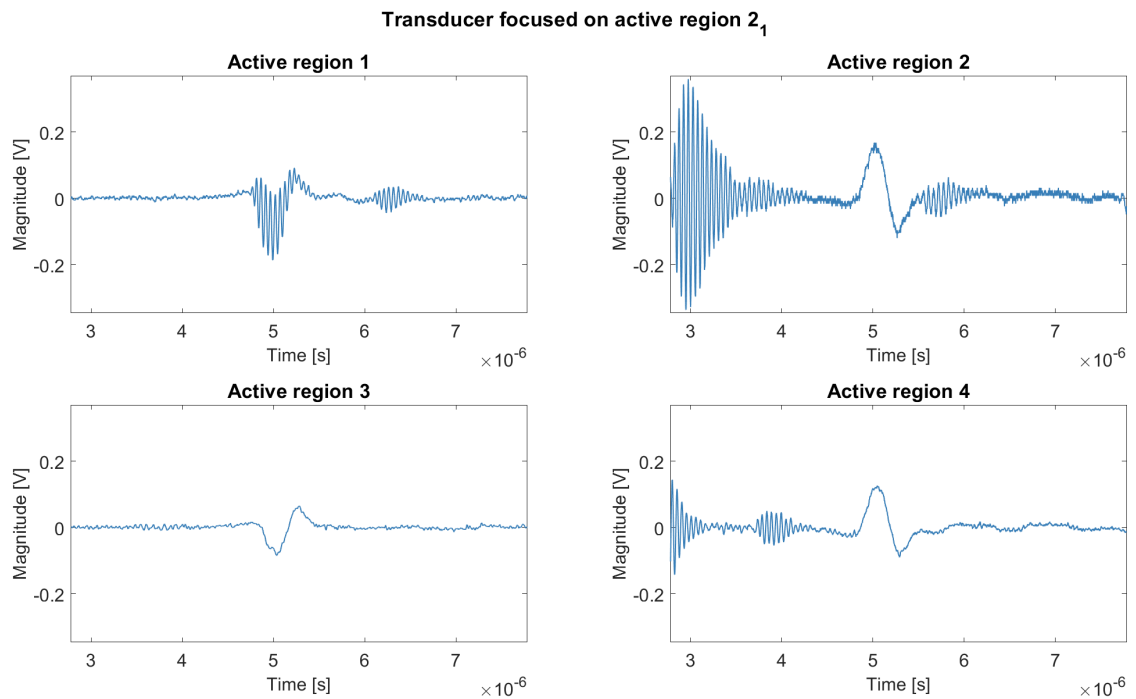


Figure B.3: Transducer focused on active region 2, rows to the signal of the BNC and columns to the ground of the BNC. The wires that aren't measured are not connected to earth.

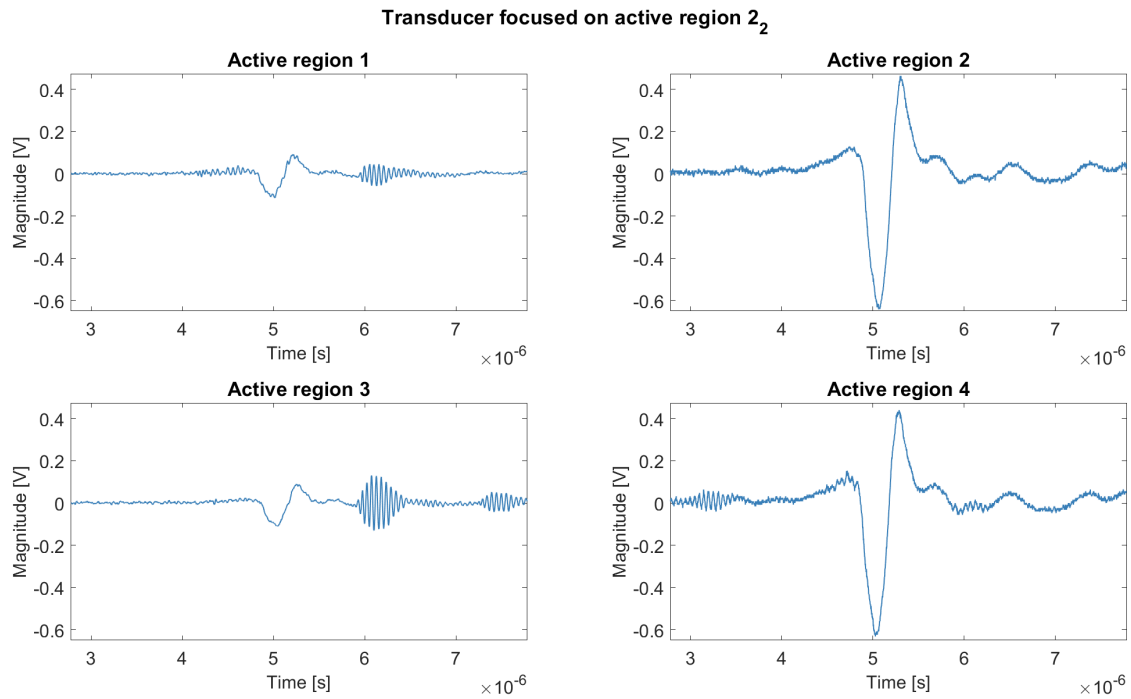


Figure B.4: Transducer focused on active region 2, columns to the signal of the BNC and rows to the ground of the BNC. The wires that aren't measured are not connected to earth

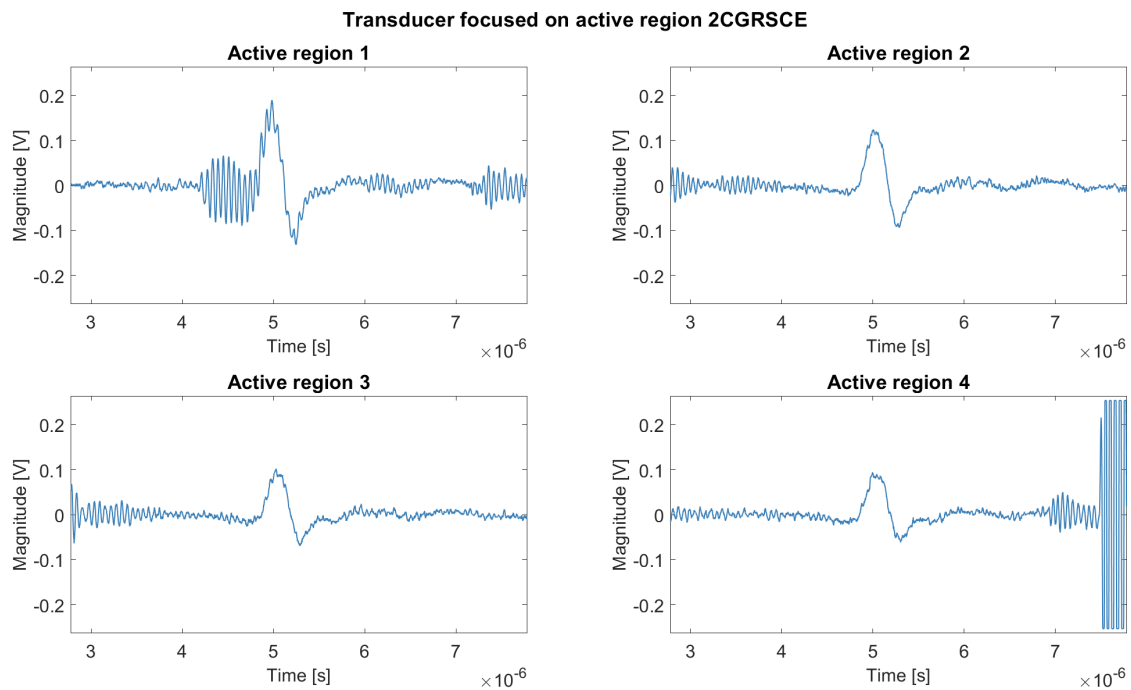


Figure B.5: Transducer focused on active region 2, columns to the ground of the BNC and rows to the signal of the BNC. Only the unmeasured columns are connected to earth

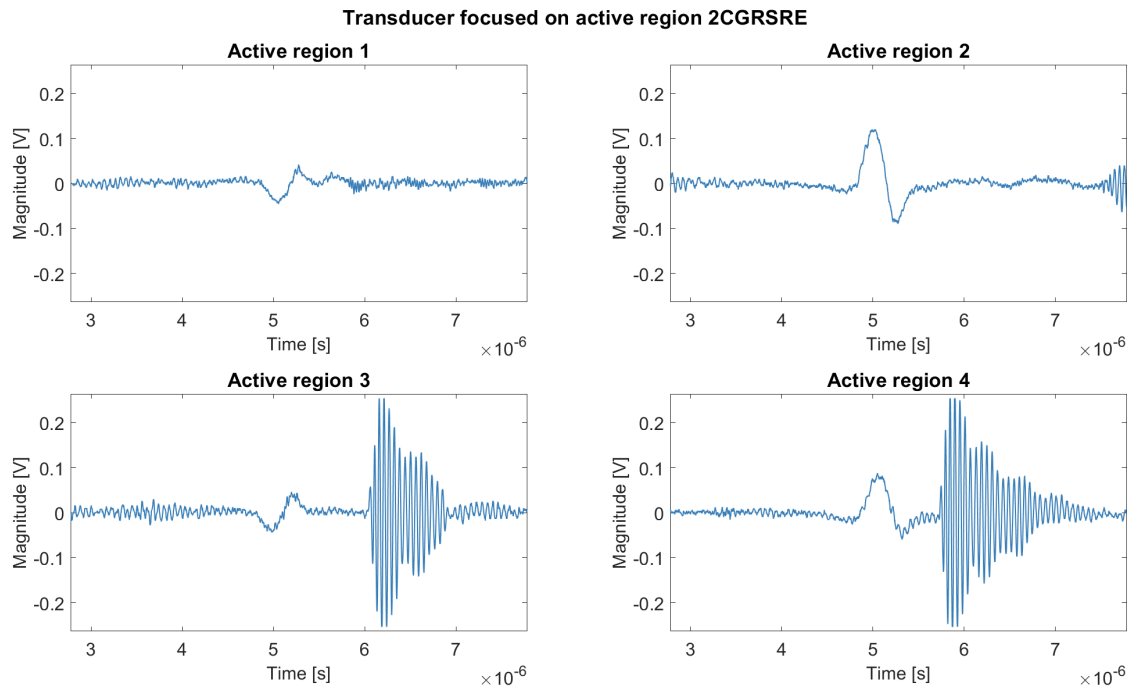


Figure B.6: Transducer focused on active region 2, columns to the ground of the BNC and rows to the signal of the BNC. Only the unmeasured rows are connected to earth

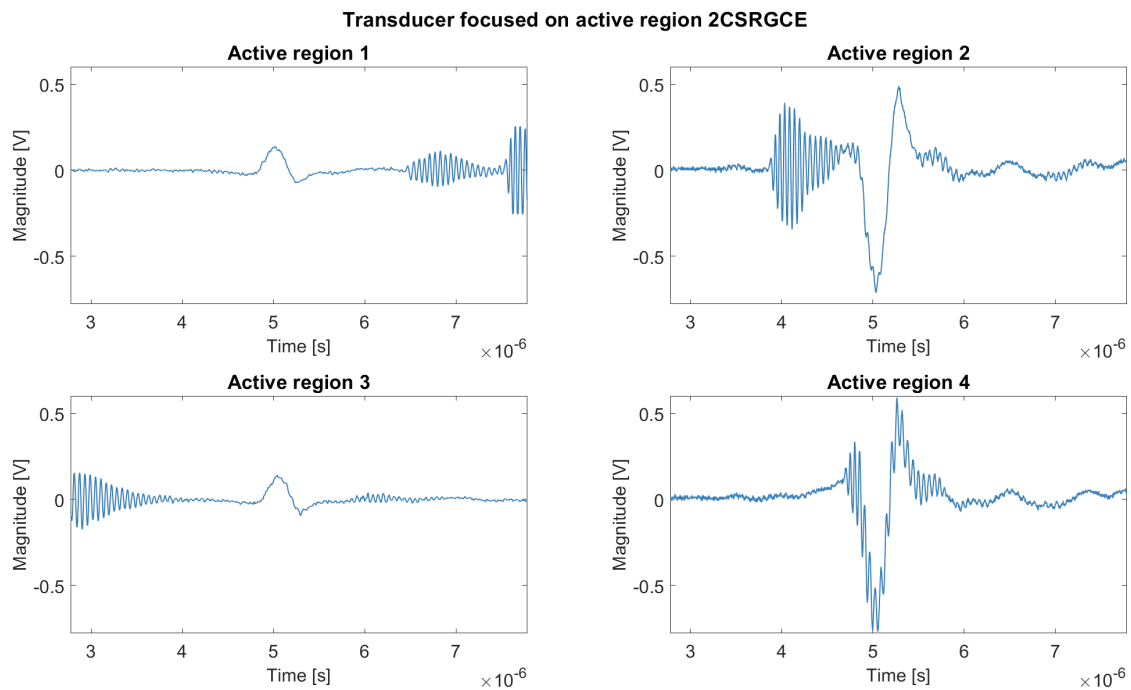


Figure B.7: Transducer focused on active region 2, columns to the signal of the BNC and rows to the ground of the BNC. Only the unmeasured columns are connected to earth

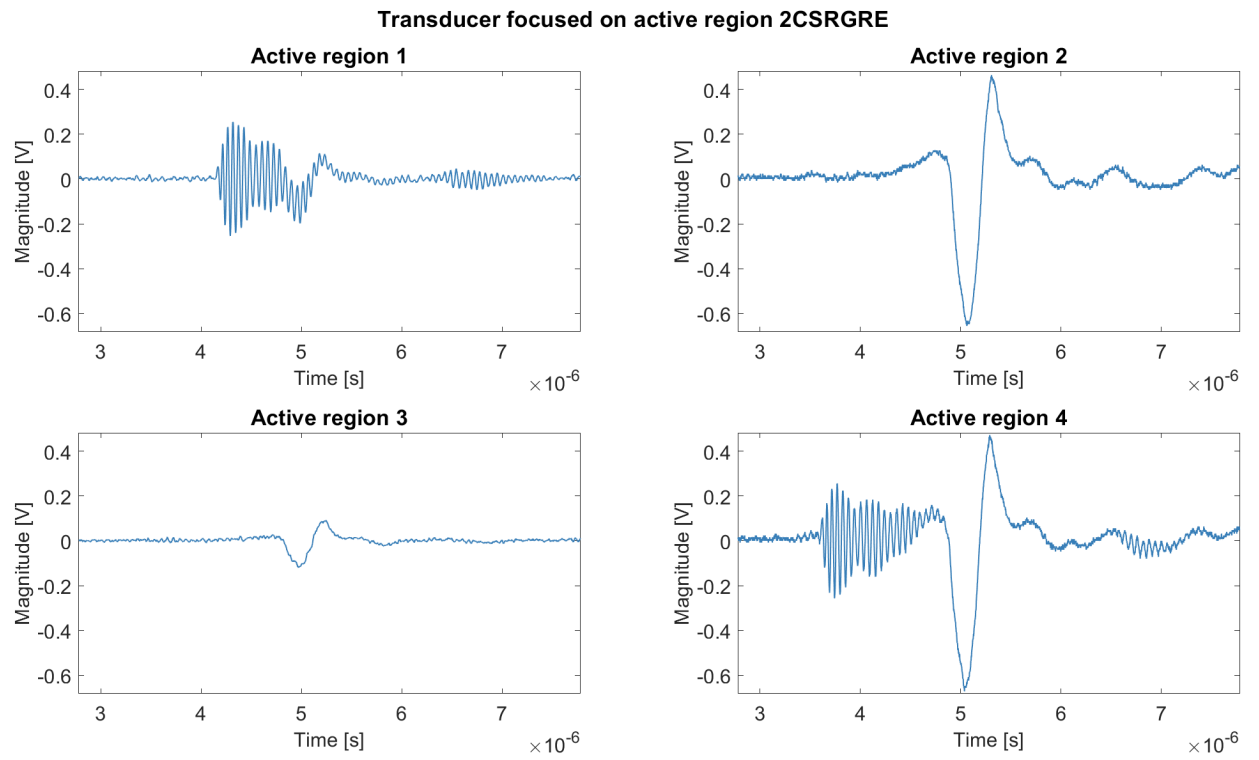


Figure B.8: Transducer focused on active region 2, columns to the signal of the BNC and rows to the ground of the BNC. Only the unmeasured rows are connected to earth

Appendix C Subtract in oscilloscope

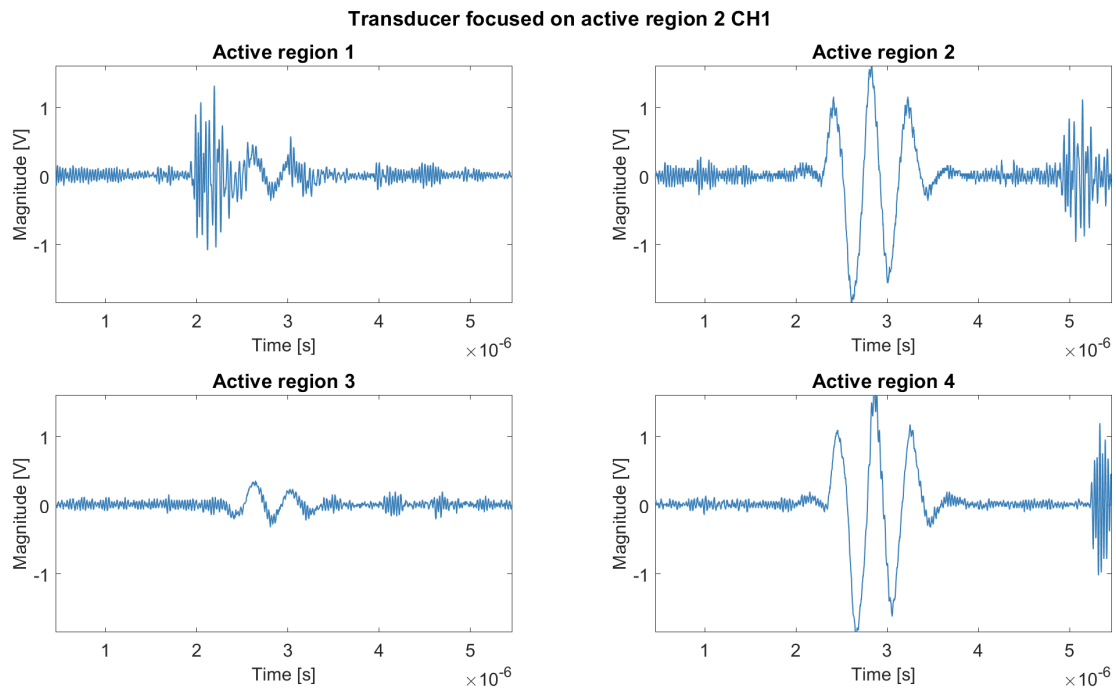


Figure C.1: Transducer focused on active region 2, signal from CH1: columns of the region of interest.

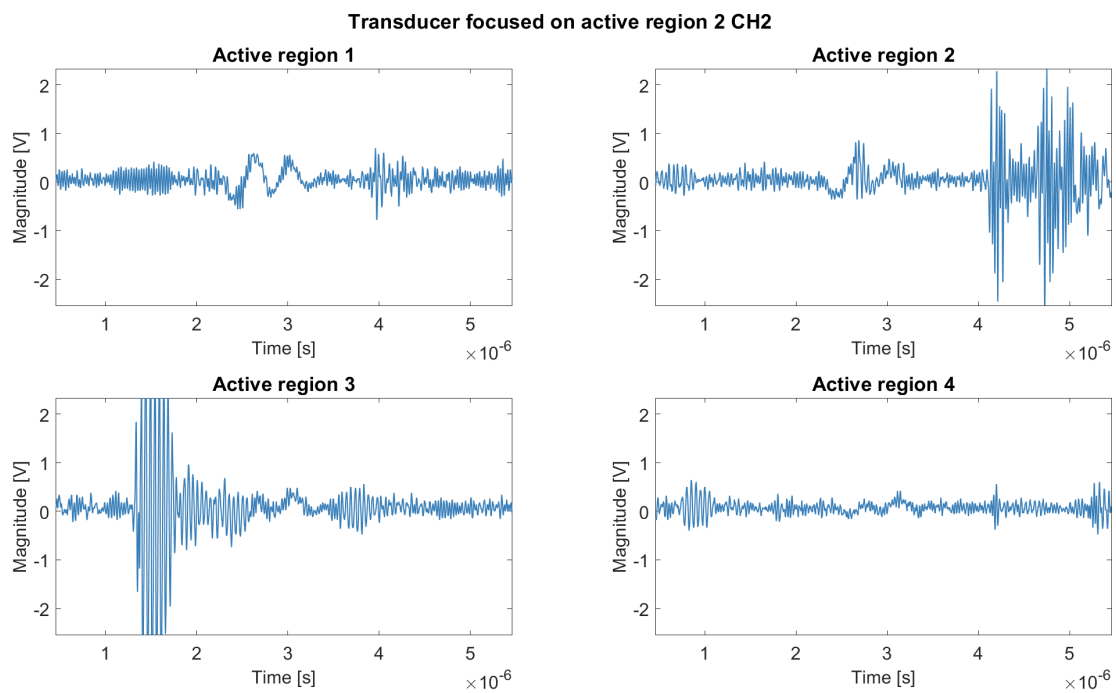


Figure C.2: Transducer focused on active region 2, signal from CH2: rows of the region of interest.

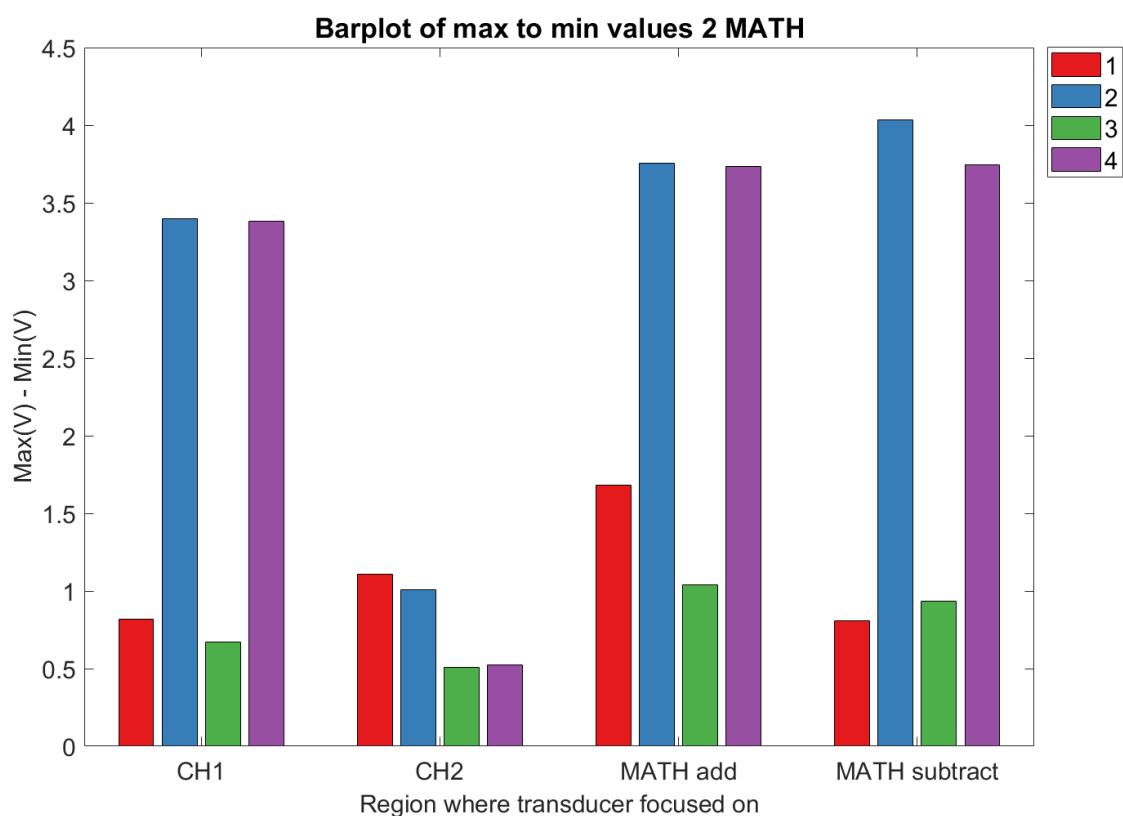
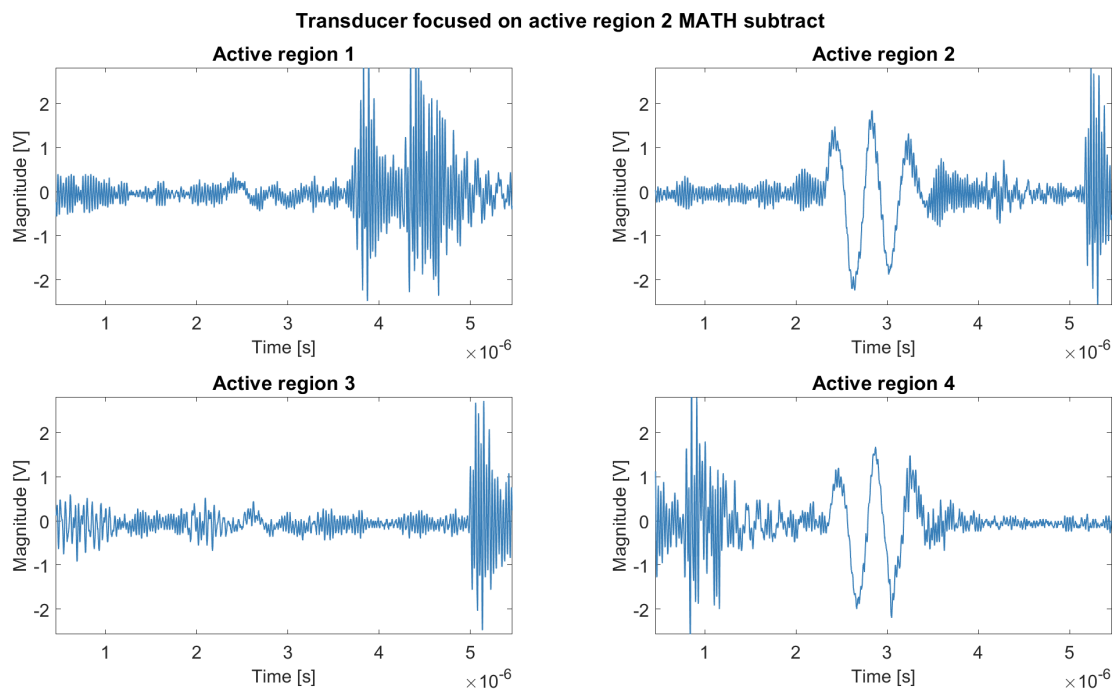


Figure C.4: Bar graph when focusing on region 2; measuring CH1, CH2, CH1 + CH2 and CH1 - CH2.

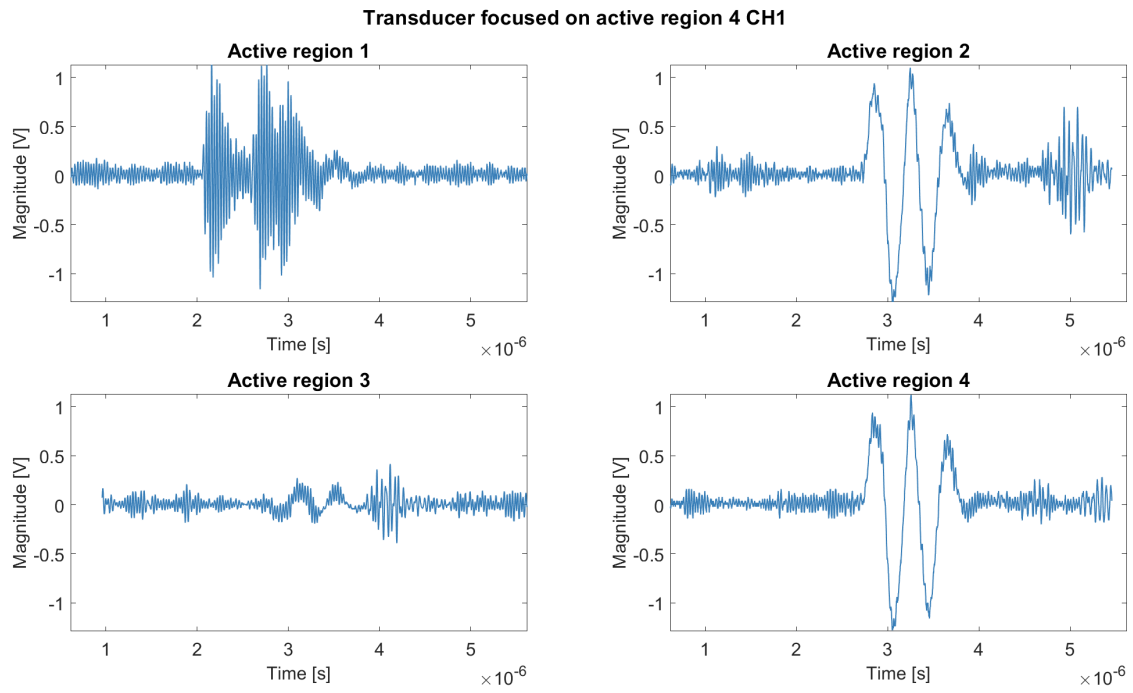


Figure C.5: Transducer focused on active region 4, signal from CH1: columns of the region of interest.

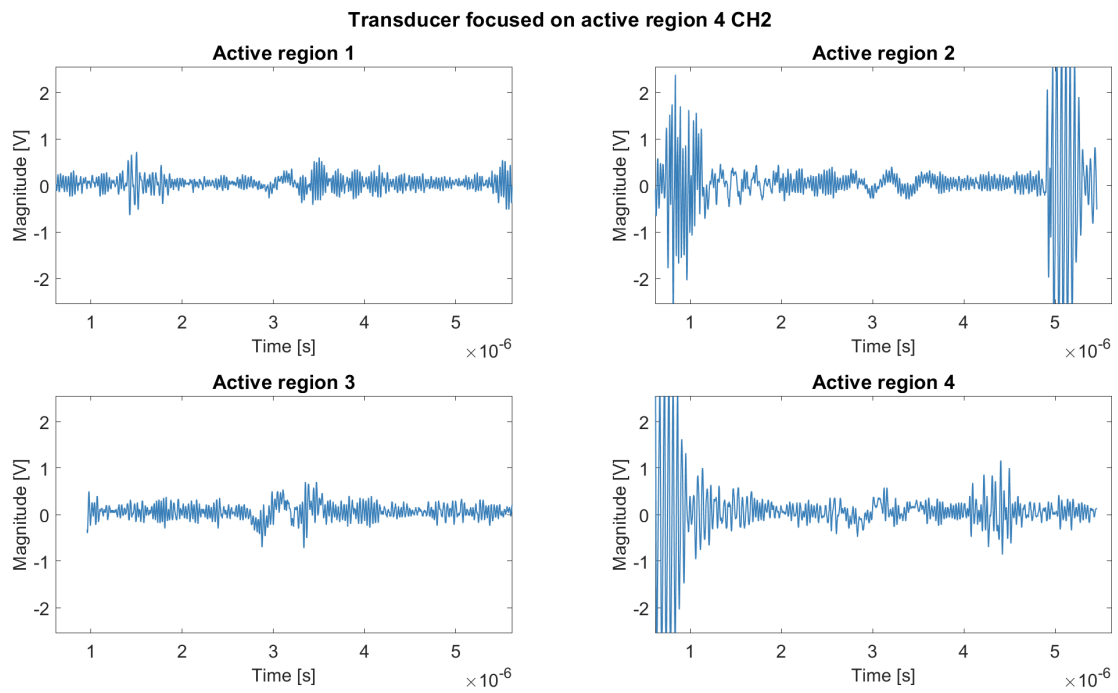


Figure C.6: Transducer focused on active region 4, signal from CH2: rows of the region of interest.

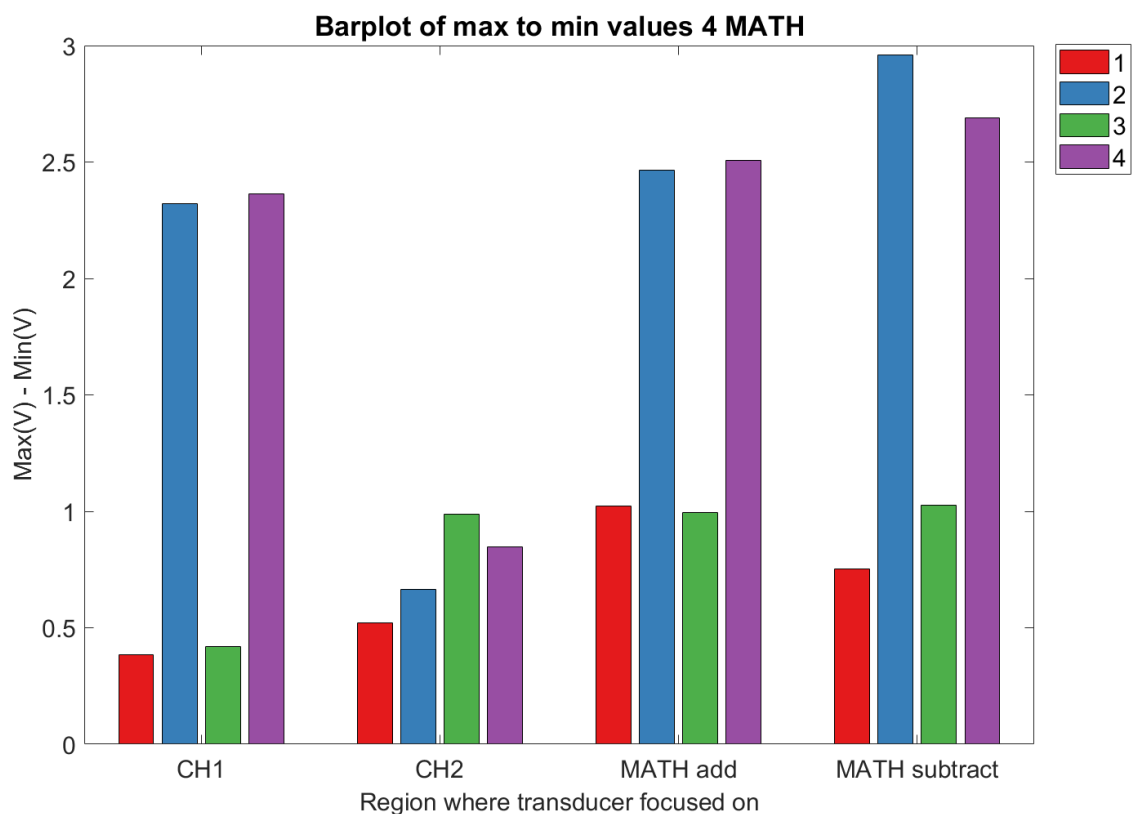
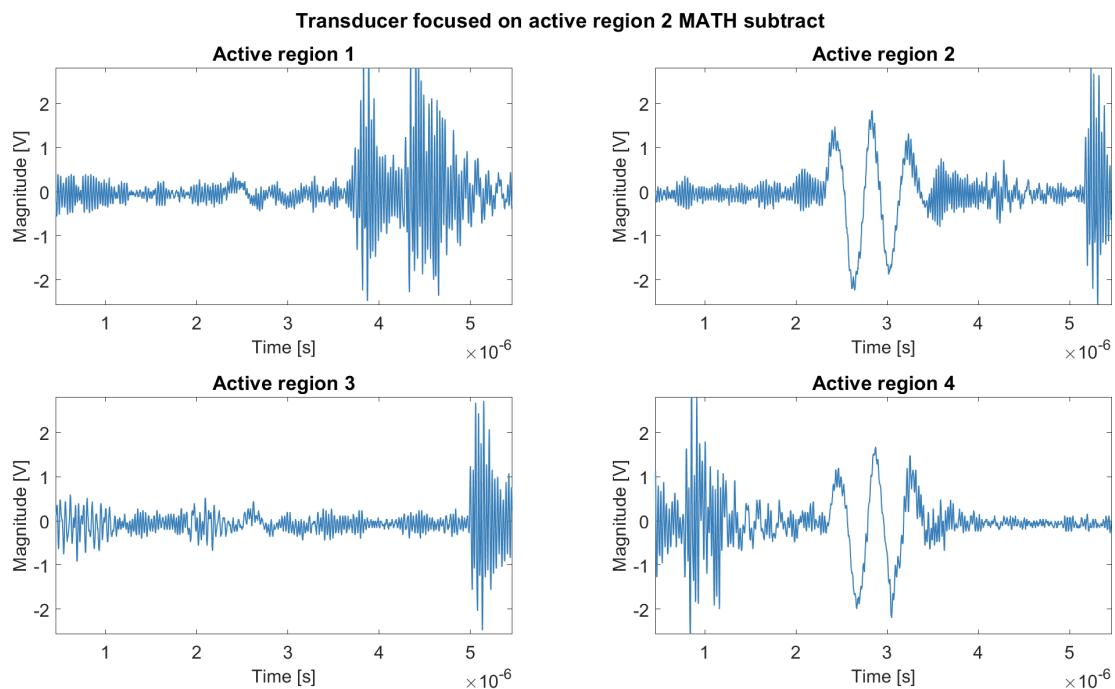


Figure C.8: Bar graph when focusing on region 4; measuring CH1, CH2, CH1 + CH2 and CH1 - CH2.

Appendix D Impedance measurement

To get a deeper understanding of how the transducer works, an impedance measurement was performed. Therefore Biologic VMP-300 was used from 2 till 7 MHz. In Figure D.1 Nyquist diagram of Prototype 1 is visible. In Figure D.2 the Nyquist diagram of Prototype 3 is visible.

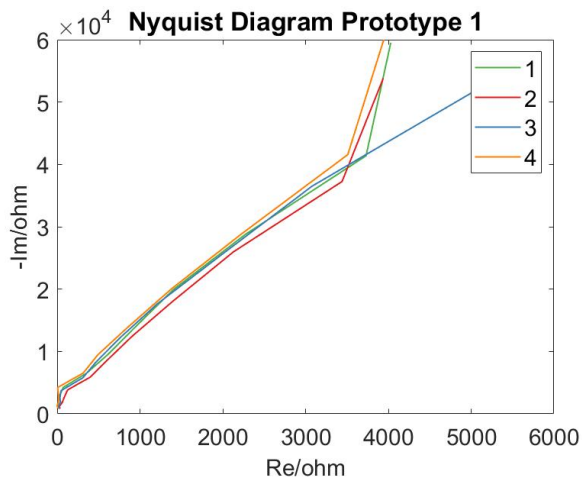


Figure D.1: Nyquist diagram for Prototype 1.

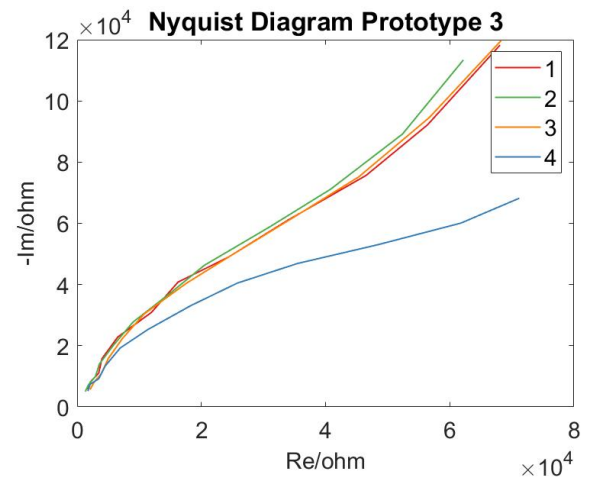


Figure D.2: Nyquist diagram for Prototype 3.